ENTANGLEMENT AND TOPOLOGICAL PHENOMENA IN QUANTUM WALKS

A Thesis Submitted to
the Graduate School of
İzmir Institute of Technology
in Partial Fulfillment of the Requirements for the Degree of

MASTER OF SCIENCE

in Physics

by
Harun GÖKALP

July 2023

İZMİR

We approve the thesis of **Harun GÖKALP**

Examining Committee Members:

Assoc. Prof. Dr. Özgür ÇAKIR
Department of Physics, İzmir Institute of Technology

Assoc. Prof. Dr. Sevilay SEVİNÇLİ
Department of Photonics, İzmir Institute of Technology

Asst. Prof. Dr. Kıvanç UYANIK
Department of Physics, Gazi University

07 / 07 / 2023

Assoc. Prof. Dr. Özgür ÇAKIR
Supervisor, Department of Physics,
İzmir Institute of Technology

Prof. Dr. Lütfi ÖZYÜZER
Head of the Department of
Physics

Prof. Dr. Mehtap EANES
Dean of the Graduate School

ACKNOWLEDGMENTS

I wish to express my sincere appreciation to my supervisor, Assoc. Prof. Dr. Özgür Çakır, for his support and help.

I also thank my family for their support and encouragement.

I must express my profound gratitude to Zülal for her unfailing support and continuous encouragement.

ABSTRACT

ENTANGLEMENT AND TOPOLOGICAL PHENOMENA IN QUANTUM WALKS

Quantum walk, a counterpart of classical random walk, is widely used in the development of quantum algorithms and the modelling of physical systems. Since it has a simple and powerful mathematical structure, its implementation in physical systems serves to solve complex problems.

In one-dimensional space, we investigated the topological properties of the simple quantum walk, and under which conditions the simple quantum walk possesses winding numbers. Then, we introduced the split-step quantum walk in a two-dimensional space and numerically obtained Chern number phase diagram of each band as a function of rotation parameters. Subsequently, we introduced and studied the quantum walk protocols governed by two coins in a two-dimensional space. We first explored the entanglement and topological properties of a quantum walk protocol governed by a single non-local two-coin operator followed by translations along two spatial directions each governed by a different coin. We deduced that the motion reduces to one-dimensional motion in two spatial directions in decoupled coin subspaces. Then, we studied the split-step quantum walk protocols, where each step is comprised of local coin operations, followed by translations, non-local coin operations, and translations again. In these protocols, each step involves two translations along two spatial directions, and translations along a given spatial direction were either governed by the same coin or alternating coins. We also explored three different non-local coin operations, where a collective rotation takes place in a coin space conditioned on the state of the other coin's state along the same direction or perpendicular direction. We identified the effective Hamiltonian of the system and determined its eigenstates which are comprised of four bands in the Brillouin zone. For all the protocols we have introduced, we studied the coin-coin entanglement and topological properties as a function of coin rotation parameters.

ÖZET

KUANTUM YÜRÜYÜŞLERDE DOLANIKLIK VE TOPOLOJİK OLGULAR

Klasik rastgele yürüyüşünün bir analojisi olarak tanımlanan kuantum yürüyüşü, kuantum algoritmalarının geliştirilmesinde ve fiziksel sistemlerin modellenmesinde sıkça kullanılmaktadır. Basit ve güçlü matematiksel yapısından dolayı fiziksel sistemlere uyarlaması kompleks problemlerin çözümüne yardımcı olur.

Bir boyutlu uzayda, basit kuantum yürüyüşünün topolojik özelliklerini ve hangi şartlar altında dolanım sayılarına sahip olduğunu inceledik. Daha sonra iki boyutlu uzayda bölünmüş-adımlı kuantum yürüyüşünü tanıttık ve her bir bandın Chern sayısı faz diyagramını döndürme parametrelerine göre nümerik olarak elde ettik. Ardından iki boyutlu bir uzayda iki kuantum parası tarafından yönetilen kuantum yürüyüş protokollerini tanıttık. İlk olarak, bir tane yerel olmayan(kolektif) kuantum parası döndürme operatöründen ve her bir yönü farklı kuantum paraları tarafından yönetilmiş öteleme operatöründen oluşan kuantum yürüyüşünün dolanıklık ve topolojik özelliklerini inceledik. Kuantum yürüyüşünün ayrıklaşmış kuantum alt uzayında bir boyutlu kuantum yürüyüşlerine indirgendiği sonucuna ulaştık. Daha sonra, her bir adımın sırasıyla yerel kuantum parası operatörlerinden, öteleme operatörlerinden, yerel olmayan kuantum parası operatöründen ve tekrar öteleme operatöründen oluşan bölünmüş-adımlı kuantum yürüyüş protokollerini inceledik. Bu protokollerde, her bir adım iki uzamsal yön boyunca iki öteleme ve aynı kuantum parası veya farklı kuantum parası tarafından yönetilen belirli bir uzamsal yön boyuncaki ötelemeleri içerir. Aynı zamanda, aynı veya dikey yön boyunca bir diğer kuantum parasının durumuna bağlı olarak kuantum parası uzayında uygulanan üç farklı yerel olmayan(kolektif) kuantum parası operatörlerini inceledik. Sistemlerin efektif Hamiltonyen'ini tanımladık ve Brillouin bölgesinde dört banttan oluşan özdurumlarını belirledik. Tanımladığımız bütün protokoller için kuantum para-kuantum para dolanıklığını ve topolojik özellikleri döndürme açılarına bağlı olarak inceledik.

TABLE OF CONTENTS

LIST OF FIGURES

LIST OF TABLES

Table **Page**

CHAPTER 1

Introduction

A classical random walk describes a random process in a mathematical space. Firstly, it is introduced by K. Pearson in order to find the probability of the walker's position after N steps on a line(Pearson, 1905). Classical random walk is a powerful tool to model and understand the behavior of complex systems due to its mathematical structure. The rigorous, formal, and the most precise explanation of random walk is given by F. Spitzer as a graduate textbook for researchers(Spitzer, 1964). The most famous example of random walk in physics is called the Brownian motion, explained by A. Einstein in 1905(Einstein, 1905). In equilibrium gas or liquid, the Brownian motion is based on the modelling of moving particles that are regarded as classical. Speaking of the Brownian motion, the term diffusion is quite related to random walk from a classical perspective. In the continuous limit, the random walk exhibits the dynamics of macroscopic diffusion. This situation means that the probability of the walker's position after large N steps forms a Gaussian distribution around the starting position of the walker, as in a diffusion process. From computer science perspective, random walk lead to the development of search algorithms by its implemented mathematical structure. The most known algorithm based on a random walk is the PageRank algorithm which seeks the importance of webpages by walking randomly among them(Page et al., 1999). The key idea beyond the algorithm is that the importance of a webpage can be understood by the number of pages linking to it.

Quantum walks, an analogy of classical random walks, are built on the principles of quantum mechanics and have applications in many fields today. The discrete-time quantum walk was first introduced in 1993 by Y. Aharonov, L. Davidovich, and N. Zagury(Aharonov et al., 1993).In quantum walks, unlike classical random walks, the walker is represented by a quantum state which consists of position and spin degree of freedom. Since interference effects exist in quantum walks, the probability of distribution of the walker does not approach a limit, unlike classical random walks(Kempe, 2003). There are two types of quantum walks: discrete-time quantum walks and continuous-time quantum walks. In discrete-time quantum walks on a lattice, each step of the walker consists of a coin-flip operator that is applied to the coin space and followed by a translation operator that depends on the walker's spin. The continuous-time quantum walk, first introduced by Farhi and Gutman in 1998, can be defined by the walker's evolution on a graph without requiring a coin-flip operator(Farhi and Gutmann, 1998). In physics, applications of quantum

walk mostly appear in the modelling and development of quantum algorithms. The first quantum algorithms, which are based on the discrete-time quantum walk, are introduced by D. Aharonov et al. and A. Ambainis et al.(Aharonov et al., 2001)(Ambainis et al., 2001). Aharonov et al. in 2001 show that the discrete-time quantum walk on a general graph can be at most polynomially faster than the classical random walk. In the work of Ambainis et al. in 2001, the authors observed several remarkable differences between quantum walk on a one-dimensional lattice and classical random walk. Following this, Shenvi et al. developed a quantum algorithm for search problems by using discrete-time quantum walk on a hypercube(Shenvi et al., 2003). In addition, Childs et al. constructed a graph and showed that the continuous-time quantum walk can be faster exponentially than classical random walk(Childs et al., 2003). J. Kempe showed that the hitting time, a fundamental concept in Markov chain theory, is exponentially faster in discrete-time quantum walk than in classical point of view(Kempe, 2005). In addition, both discrete and continuous quantum walks are the interest of research to develop universal quantum computation which defines the capacity of quantum computers to perform on arbitrary quantum systems. Separately from quantum walks, the quantum factorizing algorithm, introduced by P. Shor in 1994, is an effective algorithm that is faster than classical algorithms significantly(Shor, 1994). There are models to describe quantum computation, such as quantum circuit model, topological quantum computation, and measurement-based quantum computing. For instance, Hadamard gate is used in quantum circuit model to create the superposition between qubits. The other gates used in quantum circuit model are Pauli gates, phase gates, controlled gates, swap gates, Toffoli gate, and Fredkin gate. Lovett et al. showed quantum computation on discrete quantum walks(Lovett et al., 2010). From the perspective of physical realization, quantum walk experiments are performed using different physical systems since quantum walk cannot be restricted to specific fields(Kitagawa, 2012). One of the most known quantum walk experiments was performed with cold atoms on a line by Karski et al.(Karski et al., 2009). In the experiment, two hyperfine states of Cesium(Cs) atom were considered as spin degrees of freedom, and resonant microwave radiation was used as a spin rotation operator. The spin-dependent shift operator was implemented by continuous control of the trap polarization. The observation of quantum walk was performed up to 10 steps in the experiment. Following this, a discrete-time quantum walk experiment was implemented with single photons in space by Broome et al. in 2010(Broome et al., 2010). In this experiment, the spin degree of freedom was represented as the vertical and the horizontal polarization of the photon. Half-wave plates were used as a spin rotation operator. The spin-dependent shift operator was implemented by a birefringent calcite beam displacer. The experiment was held up to 6 steps.

Before explaining the topological aspect of quantum walks, it is essential to clarify the term topological phase in physics. The topological phase refers to quantized physical

properties and robustness against perturbations of physical systems since it cannot be defined by local parameters. The studies on topological phases have been gained an interest in condensed matter physics since the discovery of quantized Hall effect, which exhibits quantization of conductance in a two-dimensional electron gas in the existence of a strong magnetic field, by von Klitzing(Klitzing et al., 1980). With the discovery of the quantized Hall effect, topological phases have led to the invention of new materials called topological insulators(Koenig et al., 2007)(Hsieh et al., 2009).

Topological phases in the quantum walk were first introduced by T. Kitagawa, M. Rudner, E. Berg, and E. Demler in 2010(Kitagawa et al., 2010). The authors showed that stroboscopic realization of the effective Hamiltonian of the system exhibits robust topological edge states against smooth changes in rotation parameter θ. In addition to edge states, topological characterization of one-dimensional and two-dimensional quantum walks are revealed on a triangular lattice(Kitagawa et al., 2010). The first physical realization of topological phenomena in split-step quantum walks was observed with single photons generated by spontaneous parametric down conversion(Kitagawa et al., 2012). The experiment was held up to seven steps and unveiled the topological edge states by using different winding number boundaries on the lattice. In addition, the study of non-hermitian systems with parity-time symmetry by L. Xiao et al. implemented experimentally the edge states in the quantum walk by using single photons by temporally alternating photon losses(Xiao et al., 2017). The organization of the thesis is as follows:

In Chapter 1, the mathematical structure of discrete-time quantum walk is defined and investigated the probability distribution of Hadamard quantum walk to understand the behaviour of quantum walk compared to classical random walk. Then, a simple quantum walk governed by a coin is introduced to unveil the topological integer of the system in a one-dimensional lattice. Followed by the simple quantum walk, split-step quantum walk governed by a coin is defined in two-dimensional lattice and then, the definition of Chern number of the system is described and unveiled by using numerical method.

In Chapter 2, the simple quantum walk governed by two coins is introduced and discussed Chern number of the system on a two-dimensional lattice. Then, three different split-step quantum walks governed by two coins are defined by engineering appropriate unitary coin and translation operators in a two-dimensional space. Chern number phase diagram of each split-step quantum walk is obtained and discussed. Then, coin-coin entanglement of each quantum walk governed by two coins is obtained in momentum space.

1.1 Discrete-time Quantum Walk

Now, a simple example of a discrete-quantum walk can be studied by constructing mathematical and physical requirements. For a discrete-time quantum walk, Hilbert space is composed of position and coin space $\mathcal{H} = \mathcal{H}_p \otimes \mathcal{H}_C$. The position and coin space can be employed as $|j\rangle_p \in \mathcal{H}_p$ ($j = -\infty, ..., \infty$) and $|coin\rangle \in \mathcal{H}_c$ (in computational basis: $|coin\rangle \in \{|0\rangle, |1\rangle\}$), respectively. In general, the position state starts at the origin such that $|j\rangle_{initial} = |0\rangle_p$. The coin state can be described in a computational basis such that $|coin\rangle = \alpha_0 |0\rangle_c + \alpha_1 |1\rangle_c$, $|\alpha_0|^2 + |\alpha_1|^2 = 1$. For a general coin-flip operator can be chosen as a Hadamard coin operator,

$$\hat{H} = \frac{1}{\sqrt{2}} (|0\rangle \langle 0| + |0\rangle \langle 1| + |1\rangle \langle 0| - |1\rangle \langle 1|) \tag{1.1}$$

Followed by Hadamard operator, a spin-dependent translation operator can be defined on a line the following way,

$$\hat{S} = \sum_j (|j+1\rangle \langle j| \otimes |0\rangle_C \langle 0| + |j-1\rangle \langle j| \otimes |1\rangle_C \langle 1|) \tag{1.2}$$

Then, an initial state in composed Hilbert space can be defined as the following;

$$|\psi(t=0)\rangle = |0\rangle_p \otimes |coin\rangle \tag{1.3}$$

The evolution of the initial state is governed by the evolution operator of the system

$$\hat{U} = \hat{S}(\hat{I} \otimes \hat{H}) \tag{1.4}$$

The evolution of the initial state after t steps can be denoted as below;

$$|\psi(t)\rangle = \hat{U}^t |\psi(t=0)\rangle \tag{1.5}$$

By applying Hadamard operation on $|0\rangle$ and $|1\rangle$ respectively, one may extrapolate that

$$\hat{H}|0\rangle = \frac{1}{\sqrt{2}}(|0\rangle + |1\rangle) \tag{1.6}$$

$$\hat{H}|1\rangle = \frac{1}{\sqrt{2}}(|0\rangle - |1\rangle) \tag{1.7}$$

As a result from above, Hadamard operator creates an equally weighted superposition states for a chosen $|0\rangle, |1\rangle$ states initially. Followed by the Hadamard operation, spin-dependent translation operators applied on position states of the walker given by,

$$\hat{S}|0\rangle \otimes |j\rangle = |0\rangle \otimes |j+1\rangle \tag{1.8}$$

$$\hat{S}|1\rangle \otimes |j\rangle = |1\rangle \otimes |j-1\rangle \tag{1.9}$$

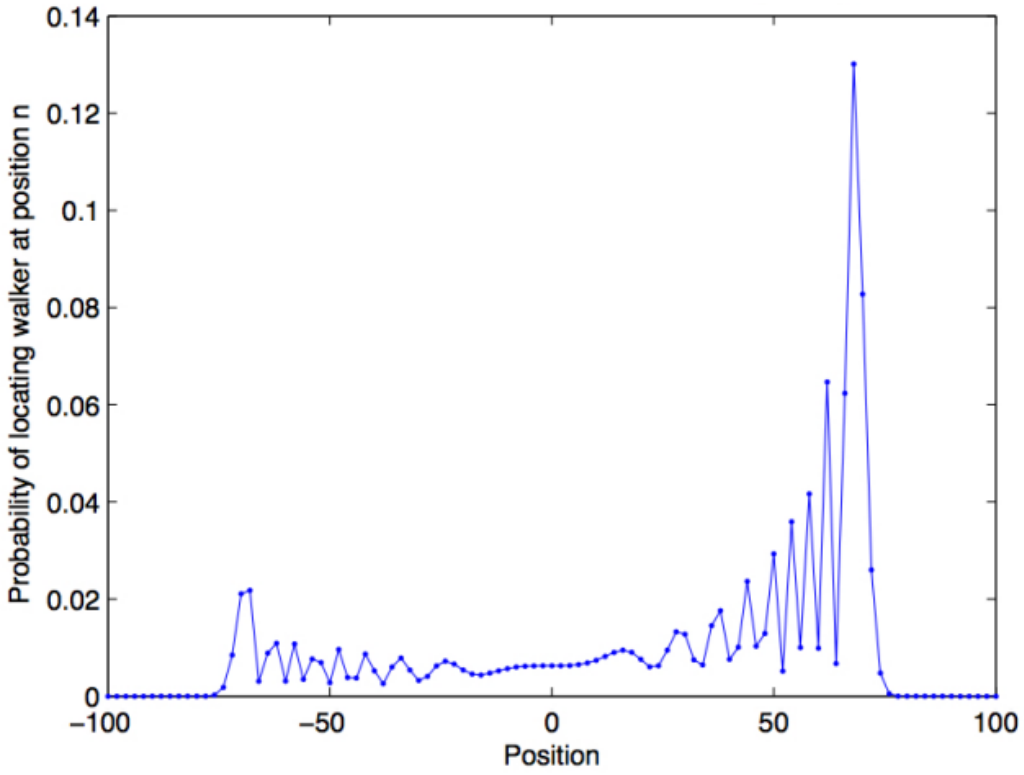

Figure 1.1: Hadamard Quantum walk of 100 steps on a line for the initial state;$|1\rangle_C \otimes |0\rangle_p$. (Venegas-Andraca, 2012)

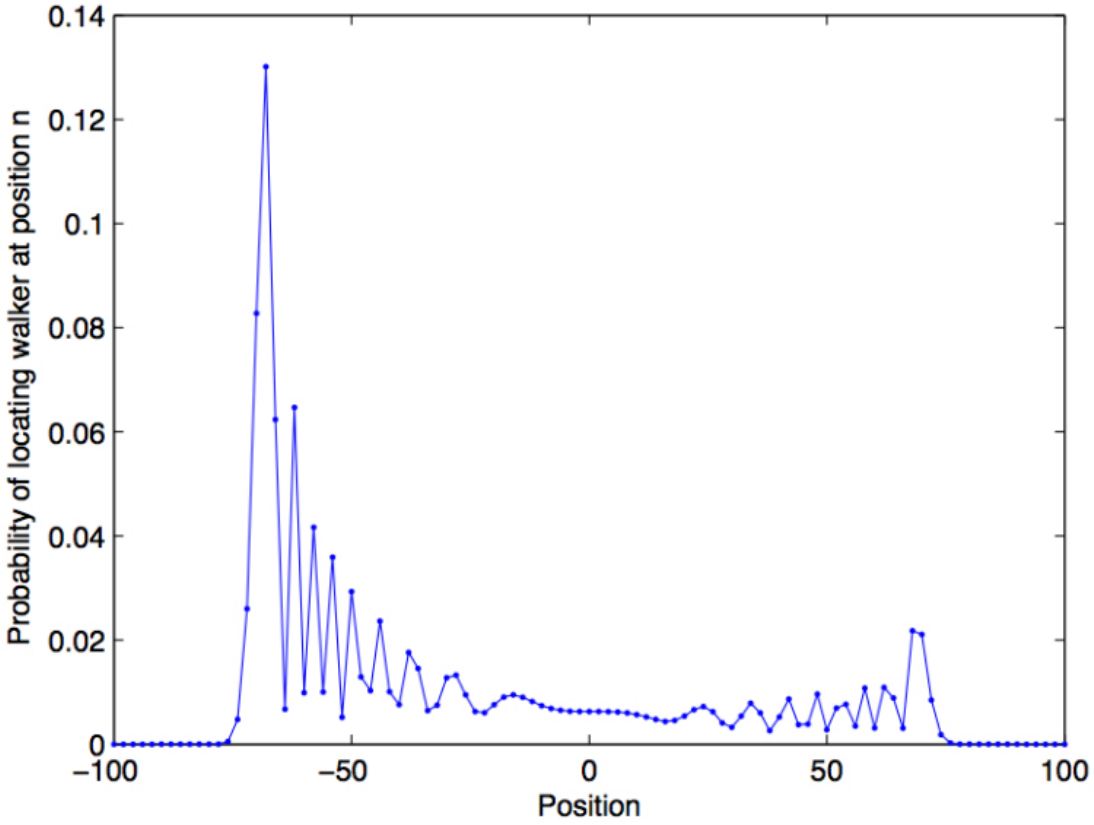

Figure 1.2: Hadamard Quantum walk of 100 steps on a line for the initial state;$|0\rangle_C \otimes |0\rangle_p$. (Venegas-Andraca, 2012)

Figures 1.1-1.2 refer to the probability distribution of Hadamard's discrete-quantum walk of 100 steps for different initial states. Asymmetry stems from the choice of the initial state, as shown in the above figures.

1.2 Simple Topological Quantum Walk In a One-Dimensional Space

Topological invariants of quantum walk protocols can be unveiled by using protocols in the seminal paper written by T. Kitagawa in 2012 (Kitagawa, 2012). In a discrete quantum walk, a quantum coin is subjected to uniter operators, such as rotation around some axis and translation through the lattice. Considering an infinite lattice from $j = -\infty$ to $j = \infty$, a discrete quantum walk protocol can be written as follows:

$$\hat{C}_y(\theta) = e^{-i\theta\sigma_y/2} \tag{1.10}$$

The operator (1.10) makes a rotation the amount of θ around $y-$ axis on the quantum coin and creates a superposition state. Then, the spin-dependent translation operator is applied to the quantum coin as below:

$$\hat{S} = \sum_{j=-\infty}^{\infty} \{|j+1\rangle \langle j| \otimes |0\rangle \langle 0| + |j-1\rangle \langle j| \otimes |1\rangle \langle 1|\} \tag{1.11}$$

As seen from (1.11), the direction in which the quantum coin moves depends on its spin. The translational operator in momentum space can be represented as,

$$\hat{S} = \int_{-\pi}^{\pi} dk e^{-ik\sigma_z} \otimes |k\rangle \langle k| \tag{1.12}$$

It is an essential realization of topological phases in momentum-space since spin information of the coin is embedded in σ_z basis (Kitagawa, 2012). Followed by the translation operator, the one-step evolution operator, $\hat{U} = e^{-i\hat{H}_{eff}\delta T}$, can be denoted as follows,

$$\hat{U} = \hat{S}\hat{C}_y(\theta) \tag{1.13}$$

Then, the stroboscopic realization of effective Hamiltonian can be written by setting $\delta T = 1$,

$$\hat{H}_{eff} = \int_{-\pi}^{\pi} dk \, (\epsilon(k)\mathbf{n}(k).\sigma) \otimes |k\rangle \langle k| \tag{1.14}$$

In closed form of Eq. (1.14), $\epsilon(k)$ and $n(k)$ represent the quasi-energy of the system and polarization of the eigenstates, respectively. The explicit form of one-step evolution

operator in momentum space is,

$$\hat{U} = \int_{FBZ} \begin{pmatrix} e^{-ik}\cos\frac{\theta}{2} & -e^{-ik}\sin\frac{\theta}{2} \\ e^{ik}\sin\frac{\theta}{2} & e^{ik}\cos\frac{\theta}{2} \end{pmatrix} dk \otimes |k\rangle\langle k| \tag{1.15}$$

To unveil the topological phase of the simple quantum walk, polarization vectors of the eigenstates, **n**(k), can be found from the explicit form of the evolution operator. The matrix notation of the effective Hamiltonian will be,

$$\hat{H}_{eff} = \int_{FBZ} \begin{pmatrix} \epsilon(k)n_z & \epsilon(k)(n_x - in_y) \\ \epsilon(k)(n_x + in_y) & -\epsilon(k)n_z \end{pmatrix} dk \otimes |k\rangle\langle k| \tag{1.16}$$

By using $\hat{U} = e^{-i\hat{H}_{eff}}$, the evolution operator in terms of $\epsilon(k)$ and $\mathbf{n}(k)$ can be written as,

$$\hat{U} = \int_{FBZ} \begin{pmatrix} \cos(\epsilon(k)) - i\sin(\epsilon(k))n_z & -i\sin(\epsilon(k))(n_x + in_y) \\ -i\sin(\epsilon(k))(n_x - in_y) & \cos(\epsilon(k)) + i\sin(\epsilon(k))n_z \end{pmatrix} dk \otimes |k\rangle\langle k| \tag{1.17}$$

Quasi-energy and polarization vectors of the system can be found by equalizing each element of operators in (1.15) and (1.17),

$$\epsilon(k) = \arccos\left(\cos\frac{\theta}{2}\cos(k)\right) \tag{1.18}$$

$$\vec{n} = \frac{1}{\sin\epsilon(k)}\left(-\sin\frac{\theta}{2}\sin k, \sin\frac{\theta}{2}\cos k, \cos\frac{\theta}{2}\sin k\right) \tag{1.19}$$

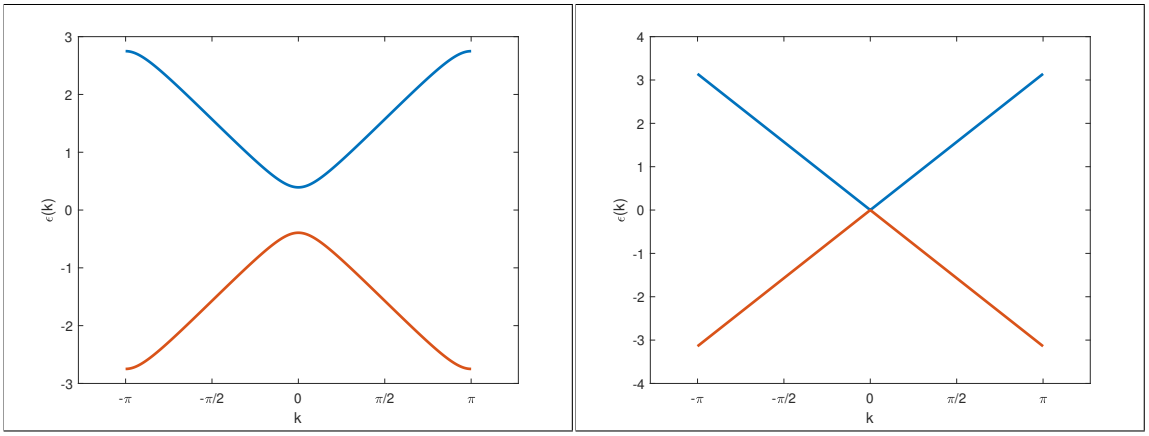

(a) Rotation angle $\theta = \frac{\pi}{4}$ (b) Rotation angle $\theta = 0$

Figure 1.3: Quasi-energy spectrum of the simple quantum walk in interval $k \in [-\pi, \pi]$ for chosen rotation parameter. In **(b)** eigenstates of the system are ill-defined since gap closes at $\theta = 0, 2\pi$.

Figure 1.3 corresponds to the quasi-energy spectrum of the simple quantum walk. In (a), the winding number of the quantum walk exists for $\theta = \frac{\pi}{4}$, whereas in (b) does not exist since the gap is closing for $\theta = 0$.

The polarization vector $\vec{\mathbf{n}}$ is a representation of eigenstates on Bloch sphere with a rotation parameter θ. It is essential to find out an axis on Bloch sphere such that $\vec{\mathbf{n}}(k).\vec{\mathbf{A}}(\theta) = 0$ at each point k since the topological phase, winding number, corresponds to turning number of $\vec{\mathbf{n}}(k)$. Then, for a chosen axis $\vec{\mathbf{A}}(\theta) = \left(\cos\frac{\theta}{2}, 0, \sin\frac{\theta}{2}\right)$, the scalar product of $\vec{\mathbf{n}}(k).\vec{\mathbf{A}}(\theta)$ equals zero for all k points. Now, the winding number of the simple quantum walk can be calculated in first Brillouin zone as the following,

$$\omega = \frac{1}{2\pi}\int_{-\pi}^{\pi} \vec{\mathbf{n}}(k).\left(d\vec{\mathbf{n}}(k) \times \vec{\mathbf{A}}(\theta)\right) \tag{1.20}$$

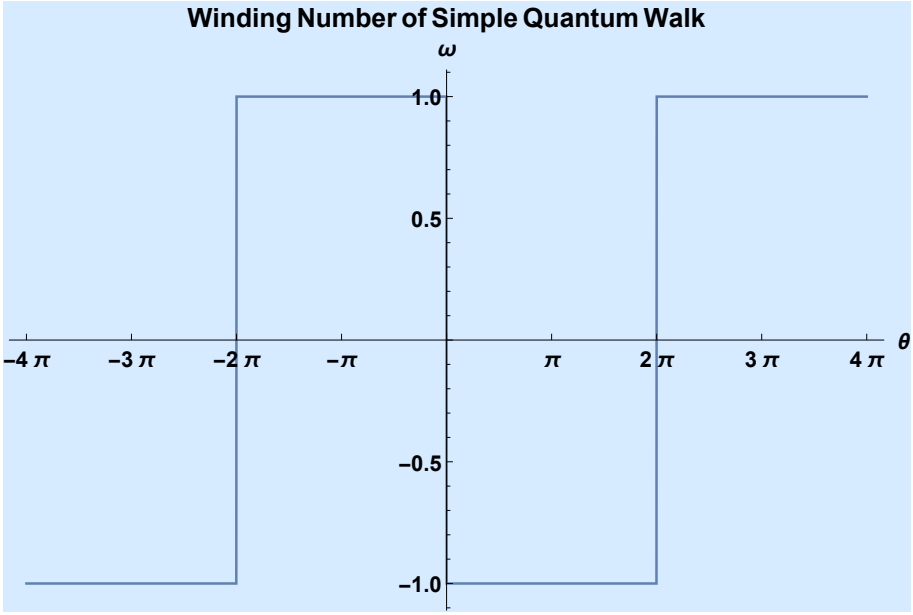

Figure 1.4: Winding number of the simple quantum walk with rotation parameter θ between $-4\pi \leq \theta \leq 4\pi$ is plotted in first Brillouin zone. As seen in the figure, winding number is indefinite for $\theta = \pm 2\pi n$, $n \in N$ due to gap is closing.

Figure 1.4 is the phase diagram of simple quantum walk in one-dimensional lattice. Since the system corresponds to a two-band effective Hamiltonian, the winding number of each eigenstate is plotted for rotation parameter θ. As seen from, the winding number of the system takes just an integer of 1 and -1 except angles corresponding to boundaries.

Another way to deduce the winding number of the system is to analyze the behavior of polarization vector $\vec{\mathbf{n}}(k)$ at lattice points $k = 0$ and $k = \pi$. The key point of the existence of winding number is directly related to the trajectory of $\vec{\mathbf{n}}(k)$ on Bloch sphere (Wang et al., 2020). At lattice points $k = 0$ and $k = \pi$, $\vec{\mathbf{n}}(0) = \frac{1}{\sin\epsilon(0)}\left(0, \sin\frac{\theta}{2}, 0\right)$ and $\vec{\mathbf{n}}(\pi) = \frac{1}{\sin\epsilon(\pi)}\left(0, -\sin\frac{\theta}{2}, 0\right)$ can be used to find out the form of trajectory.

$$\vec{\mathbf{n}}(0).\vec{\mathbf{n}}(\pi) = \frac{1}{\sin\epsilon(0)\sin\epsilon(\pi)}\left(-\sin^2\frac{\theta}{2}\right) \tag{1.21}$$

$$\vec{\mathbf{n}}(0).\vec{\mathbf{n}}(\pi) = -\frac{\sin^2\frac{\theta}{2}}{\sin^2\frac{\theta}{2}} = -1 < 0 \tag{1.22}$$

The result in Eq. (1.22) shows that vector $\vec{\mathbf{n}}(k)$ forms a closed circle on Bloch sphere. Since the sign of $\vec{\mathbf{n}}(0).\vec{\mathbf{n}}(\pi)$ is negative, the direction of $\vec{\mathbf{n}}(0)$ and $\vec{\mathbf{n}}(\pi)$ anti-parallel which means $\vec{\mathbf{n}}(\pi)$ does not return to the initial point(Wang et al., 2020). Therefore, the winding number of a chosen eigenstate is either integer of 1 or -1 in the studied simple quantum walk protocol.

1.3 Chern Number

Chern number plays an essential role in physics, particularly in the study of topological phases of matter. Chern number does not change under continuous and smooth transformations of underlying Hamiltonian. It is used to characterize the topology of the system. In physics, the quantization of Hall conductance was first introduced by Klitzing et al.(Klitzing et al., 1980). Followed by the experiment of Klitzing et al., the quantization was associated with Chern Number(Thouless et al., 1982). The quantum Hall conductance is an integer multiple of the fundamental constant $\frac{e^2}{h}$ where e is the charge of the electron, and h is Planck's constant. Chern number of the system can be calculated by using both polarization vectors and eigenstates of the Hamiltonian. In terms of polarization vectors, the calculation method of Chern number is based on the total area mapping from the first Brillouin zone to Bloch sphere such that the two-dimensional Brillouin zone corresponds to a torus that has periodic boundaries, and the number of area wrapping on Bloch sphere gives Chern number of the system(Kitagawa, 2012).

$$C = \frac{1}{4\pi} \iint_{FBZ} \mathbf{n}.\left(\frac{\partial \mathbf{n}}{\partial k_x} - \frac{\partial \mathbf{n}}{\partial k_y}\right) dk_x dk_y \tag{1.23}$$

where $\mathbf{n} = (n_x, n_y, n_z)$ and $|\mathbf{n}| = 1$. Eq. (1.23) does not explicitly indicate which energy band of the effective Hamiltonian is associated with Chern number, since polarization vectors contain information of both eigenstates. Therefore, one may use eigenstates of effective Hamiltonian to obtain Chern number of each band. By defining eigenstates $|\psi_n(\mathbf{k})\rangle = e^{i\mathbf{r}.\mathbf{k}} |\phi_n(\mathbf{k})\rangle$, Chern number of the nth band is given by;

$$C_n = \frac{1}{2\pi} \iint_{FBZ} \left(\frac{\partial A_{k_y}}{\partial k_x} - \frac{\partial A_{k_x}}{\partial k_y}\right) dk_x dk_y \tag{1.24}$$

Here, A_{k_x} and A_{k_y} correspond to Berry connection, an analogy of vector potential.

$$\begin{aligned} A_{k_x} =& i \langle \phi_n(\mathbf{k}) | \frac{\partial}{\partial k_x} | \phi_n(\mathbf{k}) \rangle \\ A_{k_y} =& i \langle \phi_n(\mathbf{k}) | \frac{\partial}{\partial k_y} | \phi_n(\mathbf{k}) \rangle \end{aligned} \tag{1.25}$$

T. Fukui et al. introduced an efficient method of numerical calculation of Chern number by discretizing the Brillouin zone using a grid in momentum space(Fukui et al., 2005). The implementation of the method in our non-degenerate systems can be denoted as follows:

1. Discretization of two-dimensional Brillouin zone:

$$\begin{aligned} k_\alpha =& (k_x, k_y) \\ (k_x, k_y) =& \left(\frac{2\pi\alpha_1}{N_1}, \frac{2\pi\alpha_2}{qN_2} \right) \end{aligned} \tag{1.26}$$

where $\alpha_1, \alpha_2 = (1, 2, ..., N_1 N_2)$. N_1, N_2 correspond to grid size of the unit cell, and q is the positive integer.

2. The infinitesimal displacement along k_x and k_y directions:

$$\begin{aligned} \hat{1} =& \frac{2\pi}{N_1}(1, 0) \longrightarrow k_x \\ \hat{2} =& \frac{2\pi}{qN_2}(0, 1) \longrightarrow k_y \end{aligned} \tag{1.27}$$

3. Definition of Link variable along k_x and k_y directions:

$$U_1(k_\alpha) = \frac{\langle \phi(k_\alpha) | \phi(k_\alpha + \hat{1}) \rangle}{|\langle \phi(k_\alpha) | \phi(k_\alpha + \hat{1}) \rangle|} \longrightarrow k_x \tag{1.28}$$

$$U_2(k_\alpha) = \frac{\langle \phi(k_\alpha) | \phi(k_\alpha + \hat{2}) \rangle}{|\langle \phi(k_\alpha) | \phi(k_\alpha + \hat{2}) \rangle|} \longrightarrow k_y \tag{1.29}$$

where $\phi(k_\alpha)$ corresponds to the Bloch function of the eigenstate underlying Hamiltonian.

4. Definition of the field strength which corresponds to Berry curvature for a unit cell in Brillouin zone:

$$F_{12}(k_\alpha) \equiv \ln \left(U_1(k_\alpha) U_2(k_\alpha + \hat{1}) U_1(k_\alpha + \hat{2})^{-1} U_2(k_\alpha)^{-1} \right) \tag{1.30}$$

5. The computation of Chern number in a two-dimensional discretized Brillouin zone:

$$C = \frac{1}{2\pi i} \sum_{k_\alpha} F_{12}(k_\alpha) \tag{1.31}$$

The numerical method provides an efficient method to avoid arbitrary gauge phases that add to eigenstates of the Hamiltonian on a two-dimensional lattice. The numerical method of Chern number is implemented to discrete quantum walk protocols to obtain a phase diagram of each band.

1.4 Split-Step Topological Quantum Walk In a Two-Dimensional Space

Split-step quantum walks are composed of multiple translations and rotation operators which depend on different rotation angles in a lattice (Kitagawa, 2012). Split-step quantum walk protocol can be defined as the following

1. First, coin tosses around the y-axis with parameter θ_1;

$$\hat{C}(\theta_1) = e^{-i\theta_1\sigma_y/2} \tag{1.32}$$

2. The conditional shift of spin up and spin down along the x and y axes;

$$\hat{S}_1 = \sum_{x,y}(|x+1, y+1\rangle \langle x, y| \otimes |0\rangle \langle 0| + |x-1, y-1\rangle \langle x, y| \otimes |1\rangle \langle 1|) \tag{1.33}$$

3. Coin tosses around the y-axis by parameter θ_2;

$$\hat{C}(\theta_2) = e^{-i\theta_2\sigma_y/2} \tag{1.34}$$

4. The conditional shift of spin up and spin down along the y-axis;

$$\hat{S}_2 = \sum_{x,y}(|x, y+1\rangle \langle x, y| \otimes |0\rangle \langle 0| + |x, y-1\rangle \langle x, y| \otimes |1\rangle \langle 1|) \tag{1.35}$$

5. Coin tosses around the y-axis by parameter θ_1;

$$\hat{C}(\theta_1) = e^{-i\theta_1\sigma_y/2} \tag{1.36}$$

6. Spin-dependent translation along the x-axis;

$$\hat{S}_3 = \sum_{x,y} \left(|x+1, y\rangle \langle x, y| \otimes |0\rangle \langle 0| + |x-1, y\rangle \langle x, y| \otimes |1\rangle \langle 1|\right) \tag{1.37}$$

The evolution operator of the system becomes,

$$\hat{U}(\theta_1, \theta_2) = \hat{S}_3\hat{C}(\theta_1)\hat{S}_2\hat{C}(\theta_2)\hat{S}_1\hat{C}(\theta_1) \tag{1.38}$$

The translation operators S_1, S_2, and S_3 can be written in momentum space the following way,

$$\hat{S}_1 = \int_{-\pi}^{\pi}\int_{-\pi}^{\pi} dk_x dk_y e^{-i(k_x+k_y)\sigma_z} \otimes \left|k_x, k_y\right\rangle \left\langle k_x, k_y\right| \tag{1.39}$$

$$\hat{S}_2 = \int_{-\pi}^{\pi} dk_y e^{-ik_y\sigma_z} \otimes \left|k_y\right\rangle \left\langle k_y\right| \tag{1.40}$$

$$\hat{S}_3 = \int_{-\pi}^{\pi} dk_x e^{-ik_x\sigma_z} \otimes |k_x\rangle \langle k_x| \tag{1.41}$$

Then, we introduce the matrix elements of the evolution operator in momentum space, explicitly;

$$\hat{U} = \iint_{FBZ} \begin{pmatrix} U_{11} & U_{12} \\ U_{21} & U_{22} \end{pmatrix} dk_x dk_y \otimes \left|k_x, k_y\right\rangle \left\langle k_x, k_y\right| \tag{1.42}$$

$$\begin{aligned}
U_{11} &= e^{-ik_x}\left(\cos\frac{\theta_2}{2}(\cos\left(k_x+2k_y\right)\cos\theta_1 - i\sin\left(k_x+2k_y\right)) - \cos(k_x)\sin\frac{\theta_2}{2}\sin\theta_1\right) \\
U_{12} &= -e^{-ik_x}\left(\sin\frac{\theta_2}{2}(\cos(k_x)\cos\theta_1 + i\sin(k_x)) + \cos\left(k_x+2k_y\right)\cos\frac{\theta_2}{2}\sin\theta_1\right) \\
U_{21} &= e^{ik_x}\left(\sin\frac{\theta_2}{2}(\cos(k_x)\cos\theta_1 - \sin(k_x)) + \cos\left(k_x+2k_y\right)\cos\frac{\theta_2}{2}\sin\theta_1\right) \\
U_{22} &= e^{ik_x}\left(\cos\frac{\theta_2}{2}(\cos\left(k_x+2k_y\right)\cos\theta_1 + i\sin\left(k_x+2k_y\right)) - \cos(k_x)\sin\frac{\theta_2}{2}\sin\theta_1\right)
\end{aligned} \tag{1.43}$$

Then,

$$\hat{U} = \iint_{FBZ} dk_x dk_y \hat{U}_{k_x,k_y} \otimes \left|k_x, k_y\right\rangle \left\langle k_x, k_y\right| \tag{1.44}$$

where $\hat{U}_{k_x,k_y}$ can be defined the following,

$$\hat{U}_{k_x,k_y} = \begin{pmatrix} \cos(\epsilon(k)) - i\sin(\epsilon(k))n_z & -i\sin(\epsilon(k))(n_x + in_y) \\ -i\sin(\epsilon(k))(n_x - in_y) & \cos(\epsilon(k)) + i\sin(\epsilon(k))n_z \end{pmatrix} \tag{1.45}$$

By Equalizing the matrix elements of (1.42) and (1.45), one gets the polarization vectors and eigen-energy function of the effective Hamiltonian as below,

$$\epsilon(k_x, k_y) = \arccos\left(\cos(k_x)\cos\left(k_x + 2k_y\right)\cos\frac{\theta_2}{2}\cos\theta_1 - \cos\frac{\theta_2}{2}\sin(k_x)\sin\left(k_x + 2k_y\right) - \cos^2(k_x)\sin\frac{\theta_2}{2}\sin\theta_1 \right) \tag{1.46}$$

$$n_x = \frac{1}{\sin(\epsilon)}\left(\sin(2k_x)\sin\frac{\theta_2}{2}\sin^2\frac{\theta_1}{2} - \cos\left(k_x + 2k_y\right)\cos\frac{\theta_2}{2}\sin(k_x)\sin\theta_1) \right) \tag{1.47}$$

$$n_y = \frac{1}{\sin(\epsilon)}\left(\left(\cos^2(k_x)\cos\theta_1 + \sin^2(k_x)\right)\sin\frac{\theta_2}{2} + \cos(k_x)\cos\left(k_x + 2k_y\right)\cos\frac{\theta_2}{2}\sin\theta_1 \right) \tag{1.48}$$

$$n_z = \frac{1}{2\sin(\epsilon)}\left(2\cos\frac{\theta_2}{2}\left(\cos\left(k_x + 2k_y\right)\cos\theta_1\sin(k_x) + \cos(k_x)\sin\left(k_x + 2k_y\right)\right) - \sin(2k_x)\sin\frac{\theta_2}{2}\sin\theta_1 \right) \tag{1.49}$$

where $\mathbf{n} = \sqrt{n_x^2 + n_y^2 + n_z^2} = 1$. Now, the quasi-energy spectrum of the split-step quantum walk can be investigated for various rotation parameters θ_1, θ_2.

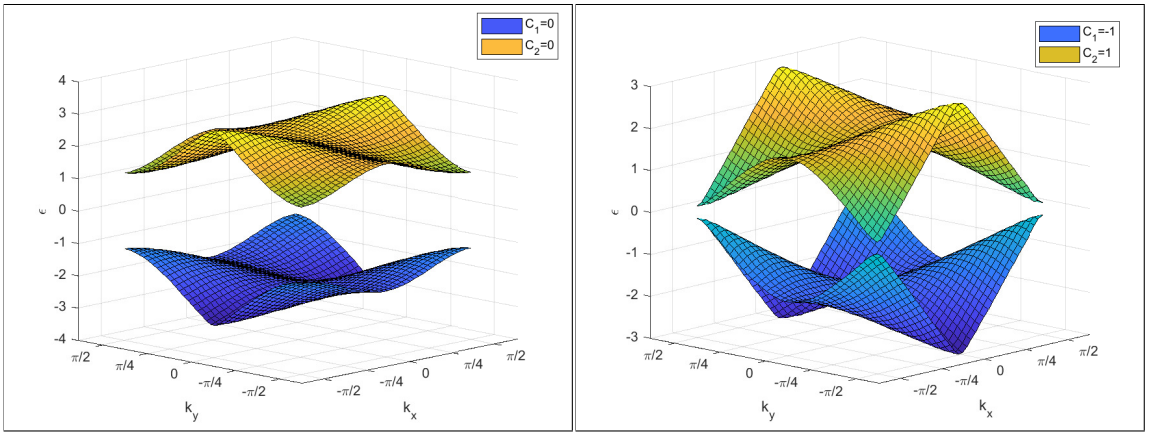

(a) Rotation angles $\theta_1 = \frac{\pi}{3}$,$\theta_2 = \frac{3\pi}{4}$ (b) Rotation angles $\theta_1 = \frac{\pi}{2}$,$\theta_2 = \frac{\pi}{11}$

Figure 1.5: The quasi-energy spectrum of two-dimensional split-step quantum walk for given rotation parameters θ_1, and θ_2 in first Brillouin zone $(k_x, k_y) \in [-\pi/2, \pi/2]$. In (a) Chern number of each band is zero, however in (b) Chern number of the system corresponds to an integer of -1, and 1.

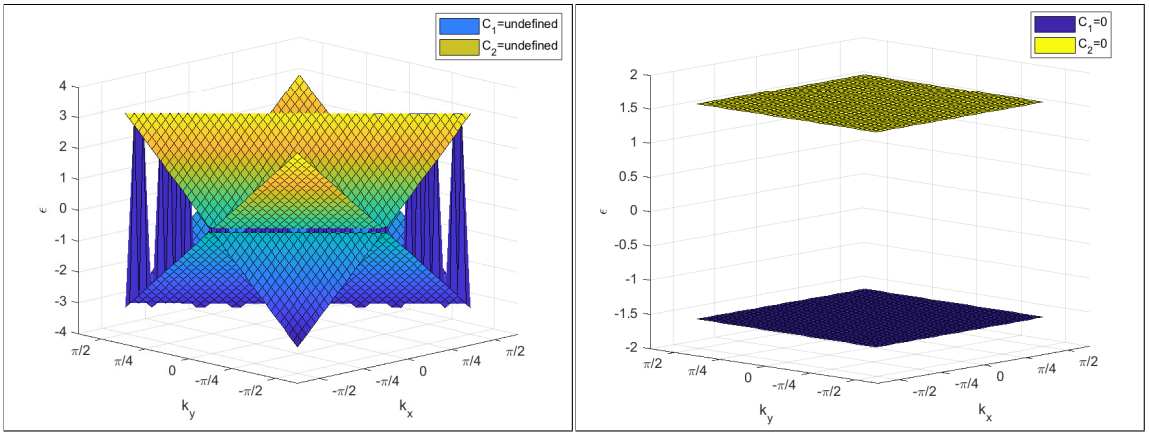

(a) Rotation angles $\theta_1 = -2\pi$,$\theta_2 = 2\pi$ (b) Rotation angles $\theta_1 = -2\pi$,$\theta_2 = \pi$

Figure 1.6: The quasi-energy spectrum of two-dimensional split-step quantum walk for given rotation parameters θ_1, and θ_2 in first Brillouin zone $(k_x, k_y) \in [-\pi/2, \pi/2]$. In (a) Chern numbers are undefined for given rotation parameters θ_1, θ_2.

Figures 1.5-1.6 represent the quasi-energy spectrum of split-step quantum walk in a two-dimensional lattice. The rotation parameters determine Chern number of the system.

Eq. (1.31) can be employed in order to investigate and analyze broadly Chern

number of the system with respect to rotation parameters θ_1, and θ_2.

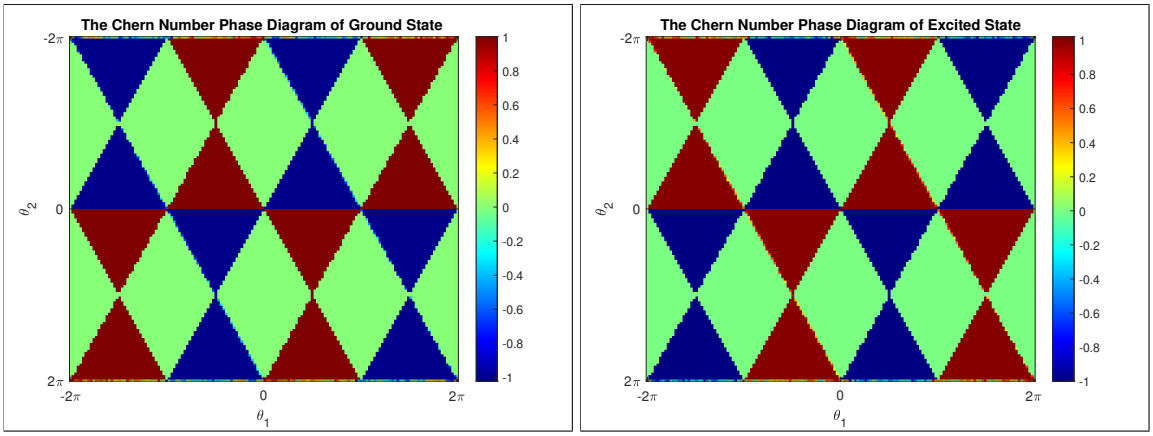

(a) Phase diagram of ground state for $(\theta_1, \theta_2) \in [-2\pi, 2\pi]$

(b) Phase diagram of excited state for $(\theta_1, \theta_2) \in [-2\pi, 2\pi]$

Figure 1.7: Numerical calculation of Chern number phase diagram of both eigenstates is plotted for rotation angles θ_1, θ_2. Chern number of split-step quantum walk in a two-dimensional lattice is associated with the integers of -1,0, and 1.

Figure (1.7) refers to Chern number phase diagram of the split-step quantum walk. In the figure, the navy blue colour corresponds to an integer of -1, while the red claret colour corresponds to an integer of 1. The green colour refers to Chern number being zero at rotation parameters. It is clear that $\sum_n C_n = 0$ except boundaries of the diagram.

In this chapter, basic preliminaries and topological aspects of quantum walks have been introduced by defining simple and split-step quantum walk protocols. To obtain topological integers, the winding number of the simple quantum walk protocol and Chern number of the two-dimensional split-step quantum walk have been calculated analytically and numerically, respectively. It is essential to realize that the winding number appears in a one-dimensional lattice while Chern number appears in a two-dimensional lattice. Since quantum walks are widely used in quantum algorithms, topological quantum walks can lead to the development of topological quantum algorithms.

CHAPTER 2

Two-Coin Topological Quantum Walk In a Two-Dimensional Space

In this chapter, we extended the quantum walks protocols by adding one more coin. We consider quantum walks on a two-dimensional lattice governed by two coins. In general, the engineered quantum walks are composed of local coin operations followed by a collective two-coin operation. Local coin operations are characterized by some rotation angle in a two-state coin space, and a non-local coin operation is a rotation in each coin space dependent on the state of the other coin. Followed by the coin operation, a displacement is made in two Cartesian directions depending on the state of the corresponding coin. The effective Hamiltonian of the system corresponds to a four-band system. The quasi-energy spectrum of the effective Hamiltonian for different rotation operators indicates how Chern numbers of the system are associated with the eigenstates of the system. Chern numbers of the systems are calculated by using Fukui's efficient algorithm on discretized Brillouin zone (Fukui et al., 2005).

2.1 Simple Quantum Walk with Two Coins

The two-coin quantum walk consists of a rotation operator and a conditional shift operator. Then, two quantum coins are labelled by Alice and Bob. Alice and Bob toss the coins respectively,

$$\mathcal{H} = \mathcal{H}_A \otimes \mathcal{H}_B \tag{2.1}$$

The following collective(non-local) coin operator makes the quantum coins entangled;

$$\hat{C}_{AB} = e^{-i\theta\sigma_x^{(A)}\otimes\sigma_x^{(B)}/2} \tag{2.2}$$

As an example, if the spin of the initial coin is $|0\rangle_A |0\rangle_B$, the final state becomes after the coin operation as below;

$$\hat{C}_{AB} |0\rangle_A |0\rangle_B = \cos(\theta/2) |00\rangle_{AB} - i \sin(\theta/2) |11\rangle_{AB} \tag{2.3}$$

Since the final state is not separable after the rotation operation, it is called an entangled state. The conditional shift operators in two-dimensional space are considered as ;

$$\begin{aligned}\hat{S}_{A_xB_y} = \sum_{x,y} &|x+1, y+1\rangle \langle x, y| \otimes |00\rangle_{AB} \langle 00|_{AB} + |x+1, y-1\rangle \langle x, y| \otimes |01\rangle_{AB} \langle 01|_{AB} \\ &+ |x-1, y+1\rangle \langle x, y| \otimes |10\rangle_{AB} \langle 10|_{AB} + |x-1, y-1\rangle \langle x, y| \otimes |11\rangle_{AB} \langle 11|_{AB}\end{aligned} \tag{2.4}$$

The translation operator in (2.4) can be factorized into one-dimension along x and y directions the following,

$$\hat{S}_{A_xB_y} = \hat{S}_{A_x} \otimes \hat{S}_{B_y} \tag{2.5}$$

According to the translation operator $\hat{S}$ in (2.4), the walker is conditionally translated diagonally along a two-dimensional space. The evolution operator of the system is $\hat{U} = e^{-iH_{eff}\delta T}$, then for $\delta T = 1$, one-step quantum walk becomes;

$$\hat{U} = \hat{S}_{A_xB_y} \hat{C}_{AB} \tag{2.6}$$

Eigen-energies of the H_{eff} define up to $\frac{2\pi}{T}$, then it is considered that H_{eff} exhibits stroboscopic feature for $\delta T = 1$ over the first Brillouin zone. The topological effects of quantum walks are observed in momentum space since the walk operator in (2.6) has translational symmetry in position space. Thus, the translation operator can be represented diagonally in momentum space ;

$$\hat{S}_{A_xB_y} = \int_{-\pi}^{\pi}\int_{-\pi}^{\pi} dk_x dk_y \left(e^{-ik_x\sigma_z^{(A)}} \otimes e^{-ik_y\sigma_z^{(B)}}\right) \otimes \left|k_x, k_y\right\rangle \left\langle k_x, k_y\right| \tag{2.7}$$

Then, the walk operator is expressed in the Brillouin zone,

$$\hat{U} = \int_{-\pi}^{\pi}\int_{-\pi}^{\pi} dk_x dk_y \hat{U}_{k_x,k_y} \otimes \left|k_x, k_y\right\rangle \left\langle k_x, k_y\right| \tag{2.8}$$

As seen from (2.7), the spin information of the coins is encoded in σ_z basis. The explicit form of $\hat{U}_{k_x,k_y}$ is ;

$$\hat{U}_{k_x,k_y} = \begin{bmatrix} e^{-i(k_x+k_y)}\cos\left(\frac{\theta}{2}\right) & 0 & 0 & -ie^{-i(k_x+k_y)}\sin\left(\frac{\theta}{2}\right) \\ 0 & e^{-i(k_x-k_y)}\cos\left(\frac{\theta}{2}\right) & -ie^{-i(k_x-k_y)}\sin\left(\frac{\theta}{2}\right) & 0 \\ 0 & -ie^{-i(-k_x+k_y)}\sin\left(\frac{\theta}{2}\right) & e^{-i(-k_x+k_y)}\cos\left(\frac{\theta}{2}\right) & 0 \\ -ie^{-i(-k_x-k_y)}\sin\left(\frac{\theta}{2}\right) & 0 & 0 & e^{-i(-k_x-k_y)}\cos\left(\frac{\theta}{2}\right) \end{bmatrix} \tag{2.9}$$

The evolution matrix of the quantum walk can be represented in different coordinates by making appropriate transformations on the first Brillouin zone. Coordinate transformation can be defined as $\frac{k_x \pm k_y}{\sqrt{2}} = k_\pm$, then the evolution operator becomes in the new coordinate

as below;

$$\hat{U}_{k_+,k_-} = \begin{bmatrix} e^{-i\sqrt{2}k_+}\cos\left(\frac{\theta}{2}\right) & 0 & 0 & -ie^{-i\sqrt{2}k_+}\sin\left(\frac{\theta}{2}\right) \\ 0 & e^{-i\sqrt{2}k_-}\cos\left(\frac{\theta}{2}\right) & -ie^{-i\sqrt{2}k_-}\sin\left(\frac{\theta}{2}\right) & 0 \\ 0 & -ie^{i\sqrt{2}k_-}\sin\left(\frac{\theta}{2}\right) & e^{i\sqrt{2}k_-}\cos\left(\frac{\theta}{2}\right) & 0 \\ -ie^{i\sqrt{2}k_+}\sin\left(\frac{\theta}{2}\right) & 0 & 0 & e^{i\sqrt{2}k_+}\cos\left(\frac{\theta}{2}\right) \end{bmatrix} \quad (2.10)$$

It is understood from (2.10), the quantum walk does not propagate in two dimensions since the eigenbasis of coin operators do not move together in k_+ and k_- directions. The bases $|00\rangle, |11\rangle$ move along the k_+ direction, and the other bases $|01\rangle, |10\rangle$ moves along the k_- direction. Therefore, the evolution operator does not possess a Chern number over first Brillouin zone since the quantum walks decompose into two different quantum walks as $\hat{U} = \hat{U}' \oplus \hat{U}''$. However, the winding number of the system can be defined for a decomposed quantum walk since each of them propagates on k_+, and k_- lines separately. As expected from the form of the evolution operator in (2.6), the band spectrum of the quantum walk exhibits degeneracy for various rotation parameter θ. By changing the order of the eigenbasis in matrix $\hat{U}$, one may find out evolution operators of the decoupled quantum walk the following,

$$\hat{U}' = \int_{-\pi}^{\pi} dk_+ \begin{pmatrix} e^{-i\sqrt{2}k_+}\cos\left(\frac{\theta}{2}\right) & -ie^{-i\sqrt{2}k_+}\sin\left(\frac{\theta}{2}\right) \\ -ie^{i\sqrt{2}k_+}\sin\left(\frac{\theta}{2}\right) & e^{i\sqrt{2}k_+}\cos\left(\frac{\theta}{2}\right) \end{pmatrix} \otimes |k_+\rangle \langle k_+| \quad (2.11)$$

$$\hat{U}'' = \int_{-\pi}^{\pi} dk_- \begin{pmatrix} e^{-i\sqrt{2}k_-}\cos\left(\frac{\theta}{2}\right) & -ie^{-i\sqrt{2}k_-}\sin\left(\frac{\theta}{2}\right) \\ -ie^{i\sqrt{2}k_-}\sin\left(\frac{\theta}{2}\right) & e^{i\sqrt{2}k_-}\cos\left(\frac{\theta}{2}\right) \end{pmatrix} \otimes |k_-\rangle \langle k_-| \quad (2.12)$$

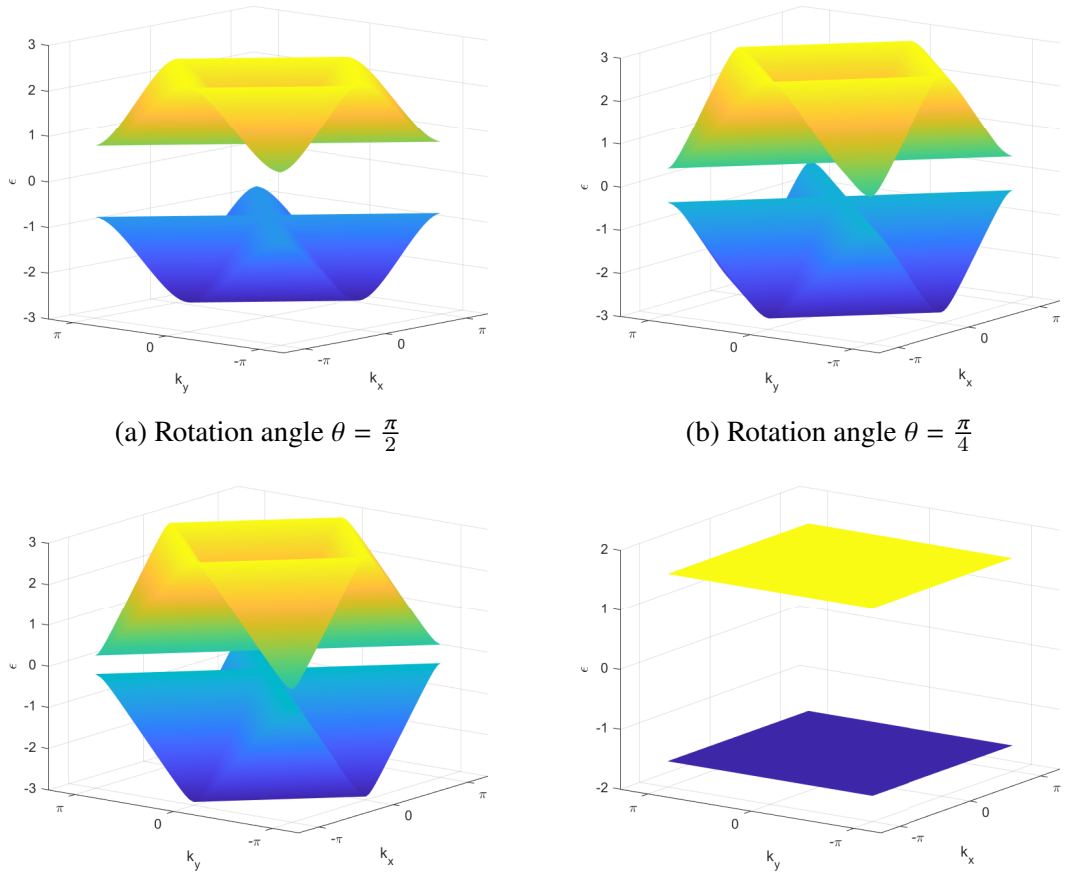

(a) Rotation angle $\theta = \frac{\pi}{2}$

(b) Rotation angle $\theta = \frac{\pi}{4}$

(c) Rotation angle $\theta = \frac{\pi}{7}$

(d) Rotation angle $\theta = \pi$

Figure 2.1: The band spectrum of effective Hamiltonian for various rotation angles θ in first Brillouin zone $k_{x,y} \in [-\pi, \pi]$. The system exhibits a degeneracy at each rotation parameter θ.

Figure 2.1 shows that the decoupling of the simple quantum walk occurs for chosen rotation parameters. Since the quantum walk does not propagate in two-dimensional the Brillouin zone, Chern numbers of each band are undefined.

The winding number of each decoupled quantum walk can be calculated by using Eq. (1.20) since the quantum walk operator in (2.6) is effectively separated into one-dimensional quantum walks in position space.

2.2 Split-Step Quantum Walks with Two Coins

Table 2.1: The studied split-step quantum walk protocols. Each protocol consists of different non-local coin operators and translation operators.

Protocol List			
Protocol Number	Quantum Walk Operator	Non-Local Operators	Local Coin Operators
Model 1	$\hat{S}_{A_xB_y}\hat{C}_{AB}\hat{S}_{B_x}\hat{C}_B\hat{S}_{A_y}\hat{C}_A$	$\hat{C}_{AB} = e^{-i\theta_3\sigma_x^{(A)}\otimes\sigma_x^{(B)}/2}$	$\hat{C}_A = e^{-i\theta_1\sigma_x^{(A)}/2}$ $\hat{C}_B = e^{-i\theta_2\sigma_x^{(B)}/2}$
Model 2	$\hat{S}_{A_xB_y}\hat{C}_{AB}\hat{S}_{B_y}\hat{C}_B\hat{S}_{A_x}\hat{C}_A$	$\hat{C}_{AB} = e^{-i\theta_3\sigma_y^{(A)}\otimes\sigma_y^{(B)}/2}$	$\hat{C}_A = e^{-i\theta_1\sigma_x^{(A)}/2}$ $\hat{C}_B = e^{-i\theta_2\sigma_x^{(B)}/2}$
Model 3	$\hat{S}_{A_xB_y}\hat{C}_{AB}\hat{S}_{B_x}\hat{C}_B\hat{S}_{A_y}\hat{C}_A$	$\hat{C}_{AB} = e^{-i\theta_3\sigma_z^{(A)}\otimes\sigma_y^{(B)}/2}$	$\hat{C}_A = e^{-i\theta_1\sigma_x^{(A)}/2}$ $\hat{C}_B = e^{-i\theta_2\sigma_x^{(B)}/2}$

The split-step quantum walks are composed of three simple quantum walks. The study of split-step quantum walks provides the observation of topological effects on the first Brillouin Zone. Unlike the simple quantum walk in (2.6), decoupling of the eigenbasis does not occur in split-step quantum walk. The lattice constant of the quantum walk corresponds to 2 unit cell in the two-dimensional lattice, since the translation operators are applied on the walker along the x, y-directions more than once. In momentum representation, periodicity of the effective Hamiltonian is $\frac{\pi}{2}$ and first Brillouin zone defines a torus with boundaries $k_x, k_y \in [-\frac{\pi}{2}, \frac{\pi}{2}]$. Boundaries of the first Brillouin zone are vital since the calculation of Chern number over the first Brillouin zone is based on the turning number of the eigenstates of the effective Hamiltonian.

2.2.1 The First Split-Step Quantum Walk Protocol

The following unitary operators define our first split-step quantum walk in the Hilbert space,

1. Alice tosses the first coin around x-axis;

$$\hat{C}_A = e^{-i\theta_1 \sigma_x^{(A)}/2} \tag{2.13}$$

2. The conditional shift operator is defined on the walker along the y-axis;

$$\hat{S}_{A_y} = \sum_y \{|y+1\rangle \langle y| \otimes |0\rangle_A \langle 0|_A + |y-1\rangle \langle y| \otimes |1\rangle_A \langle 1|_A\} \tag{2.14}$$

3. Bob tosses the second coin around x-axis;

$$\hat{C}_B = e^{-i\theta_2 \sigma_x^{(B)}/2} \tag{2.15}$$

4. After the coin tossing, the shift operator along the x-axis is;

$$\hat{S}_{B_x} = \sum_x \{|x+1\rangle \langle x| \otimes |0\rangle_B \langle 0|_B + |x-1\rangle \langle x| \otimes |1\rangle_B \langle 1|_B\} \tag{2.16}$$

5. A non-local(collective) coin operator is introduced along the x direction;

$$\hat{C}_{AB} = e^{-i\theta_3 \sigma_x^{(A)} \otimes \sigma_x^{(B)}/2} \tag{2.17}$$

6. Followed by the non-local coin operation, a displacement is made in two Cartesian directions;

$$\hat{S}_{A_xB_y} = \sum_{x,y} |x+1, y+1\rangle \langle x, y| \otimes |00\rangle_{AB} \langle 00|_{AB} + |x+1, y-1\rangle \langle x, y| \otimes |01\rangle_{AB} \langle 01|_{AB} + |x-1, y+1\rangle \langle x, y| \otimes |10\rangle_{AB} \langle 10|_{AB} + |x-1, y-1\rangle \langle x, y| \otimes |11\rangle_{AB} \langle 11|_{AB} \quad (2.18)$$

The first split-step quantum walk protocol can be denoted as ;

$$\hat{U}^{(1)} = \hat{S}_{A_xB_y} \hat{C}_{AB} \hat{S}_{B_x} \hat{C}_B \hat{S}_{A_y} \hat{C}_A \quad (2.19)$$

Chern numbers of split-step quantum walks are numerically calculated by using Eq. (1.31). For the protocol $\hat{U}^{(1)}$, eigenstates and quasi-energies of the effective Hamiltonian can be represented the following,

$$\hat{U}^{(1)} = \int_{-\frac{\pi}{2}}^{\frac{\pi}{2}} \int_{-\frac{\pi}{2}}^{\frac{\pi}{2}} e^{-i\epsilon_n(k_x,k_y)} \left|\phi_n(k_x, k_y)\right\rangle \left\langle\phi_n(k_x, k_y)\right| dk_x dk_y \otimes \left|k_x, k_y\right\rangle \left\langle k_x, k_y\right| \quad (2.20)$$

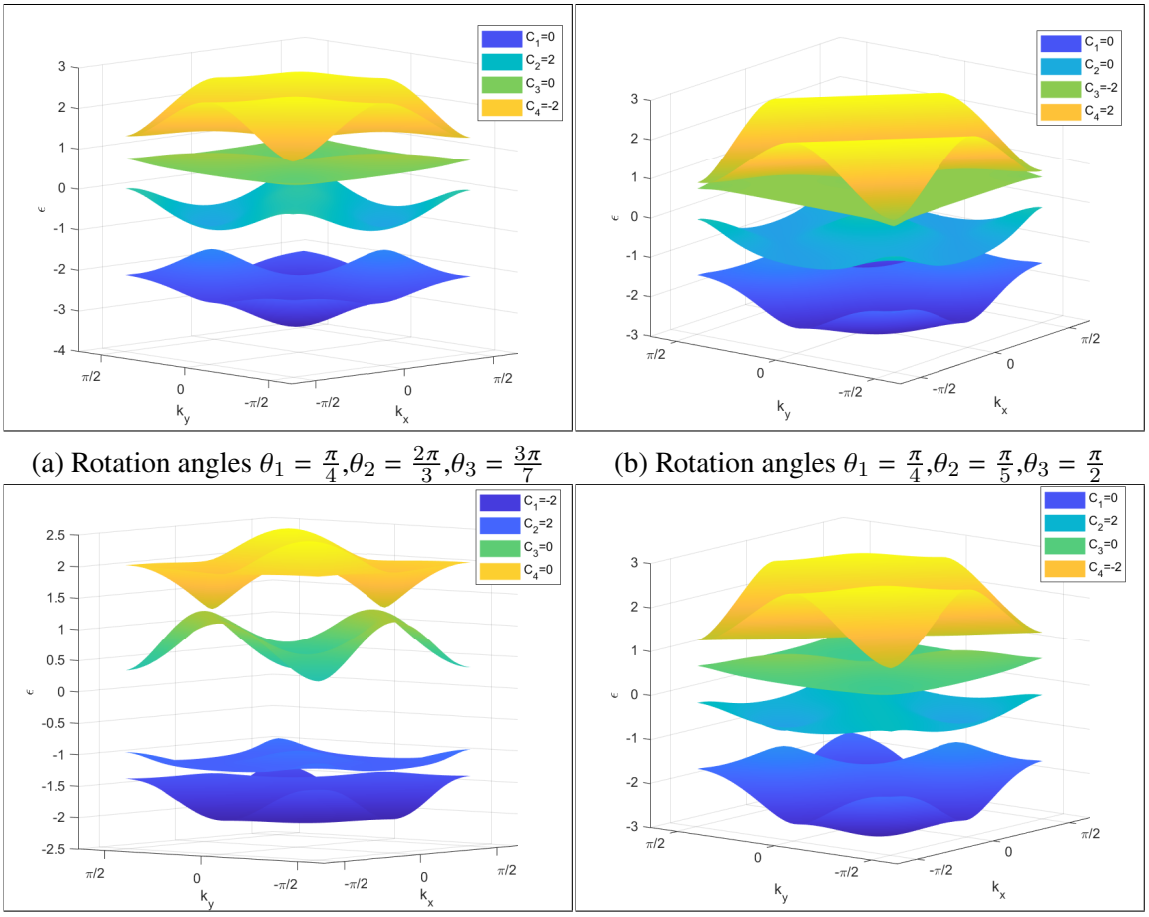

(a) Rotation angles $\theta_1 = \frac{\pi}{4}$,$\theta_2 = \frac{2\pi}{3}$,$\theta_3 = \frac{3\pi}{7}$

(b) Rotation angles $\theta_1 = \frac{\pi}{4}$,$\theta_2 = \frac{\pi}{5}$,$\theta_3 = \frac{\pi}{2}$

(c) Rotation angles $\theta_1 = \frac{-\pi}{3}$, $\theta_2 = \frac{-\pi}{5}$, $\theta_3 = \frac{-3\pi}{4}$

(d) Rotation angles $\theta_1 = \frac{\pi}{7}$,$\theta_2 = \frac{3\pi}{5}$,$\theta_3 = \frac{\pi}{3}$

Figure 2.2: The quasi-energy spectrum of the first split-step quantum walk protocol for various rotation angles θ_1,θ_2, and θ_3 in the first Brillouin zone $k_{x,y} \in [-\pi/2, \pi/2]$.

Figure 2.2 represents the quasi-energy spectrum of the first split-step quantum walk protocol with different rotation parameters. As seen in the figure, the eigenstates of the effective Hamiltonian are well-defined for given rotation parameters. Thus, the system possesses Chern number over the first Brillouin zone.

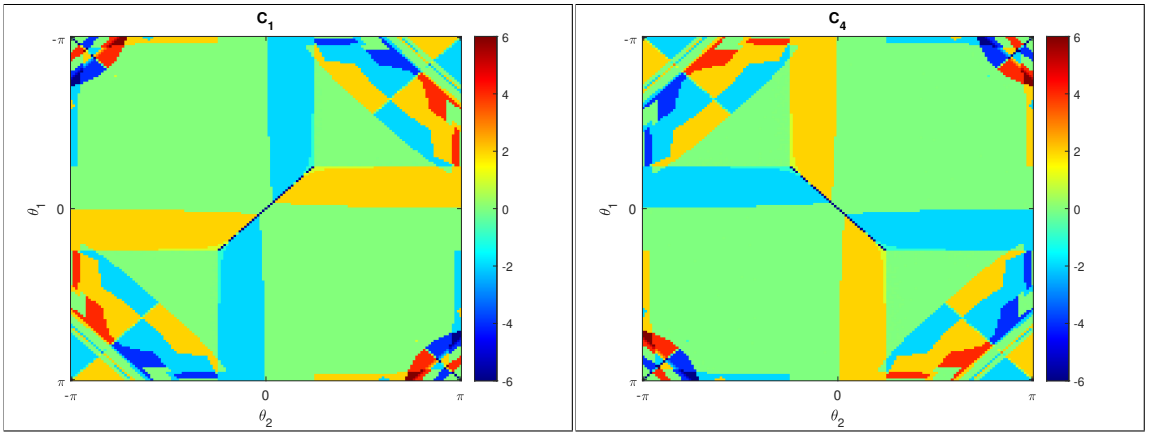

(a) Rotation angle $\theta_3 = \frac{\pi}{4}$ (b) Rotation angle $\theta_3 = \frac{\pi}{4}$

Figure 2.3: Chern number phase diagram of the first split-step quantum walk protocol is plotted for the ground state and the third excited state in the interval of $\theta_1, \theta_2 \in [-\pi, \pi]$.

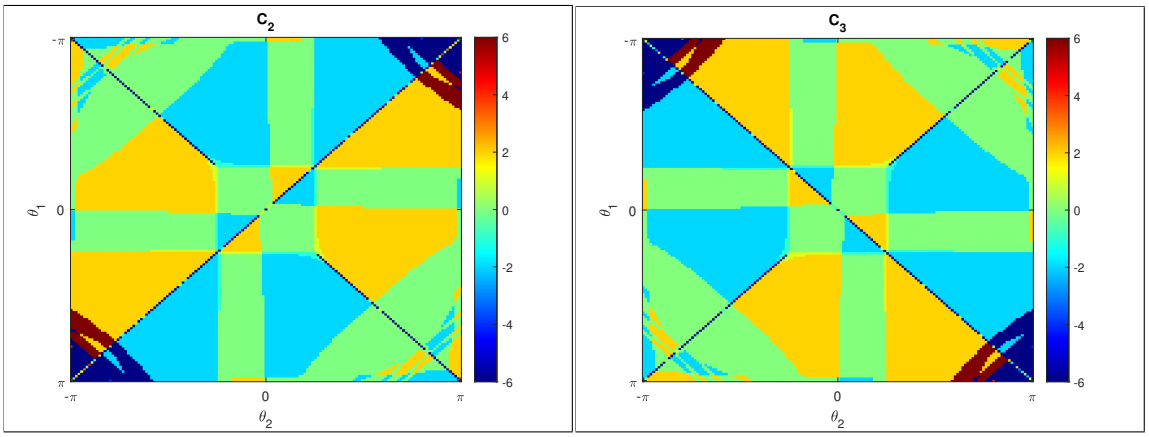

(a) Rotation angle $\theta_3 = \frac{\pi}{4}$ (b) Rotation angle $\theta_3 = \frac{\pi}{4}$

Figure 2.4: Chern number phase diagram of the first split-step quantum walk protocol is plotted for the first excited state and the second excited state in the interval of $\theta_1, \theta_2 \in [-\pi, \pi]$.

Figures 2.3-2.4 contain Chern number phase diagram of each band with constant rotation parameter θ_3, and indicate how Chern numbers change with respect to rotation parameters θ_1, θ_2. As seen from the figures, each band is mostly characterized by integers of $-2, 0, 2$. The colours aqua, green, and orange correspond to integers of $-2, 0, 2$, respectively.

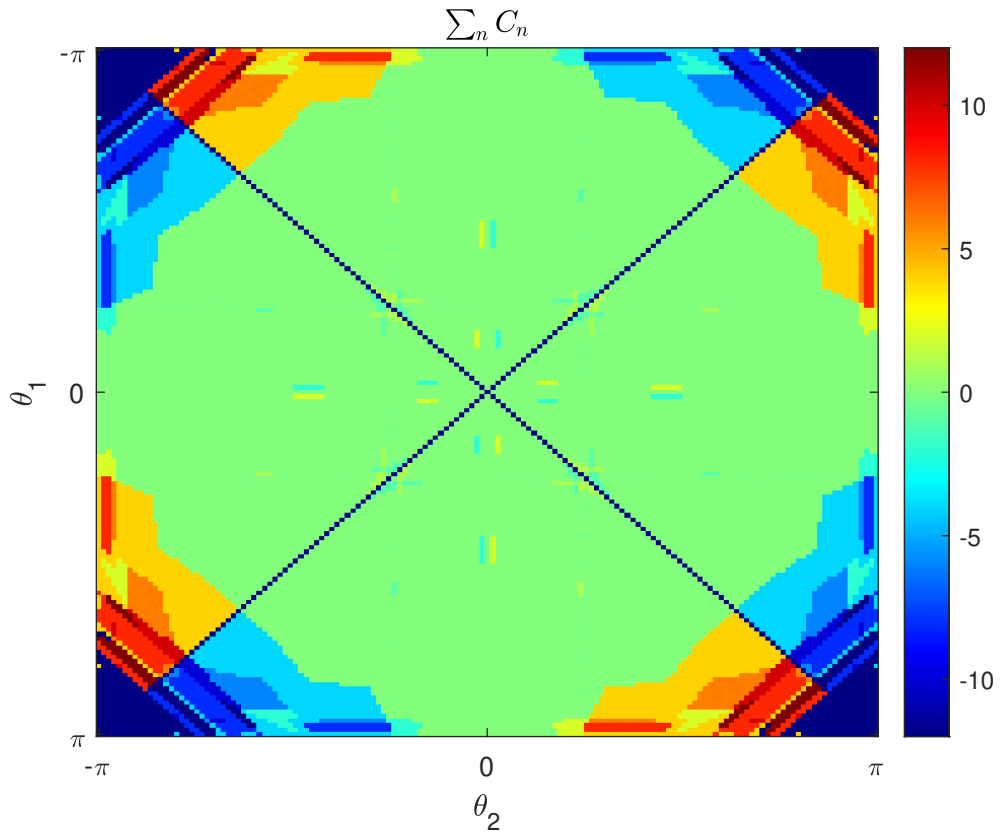

Figure 2.5: Summation of Chern number phase diagrams of all bands with constant rotation parameter $\theta_3 = \frac{\pi}{4}$ is plotted in interval of $\theta_1, \theta_2 \in [-\pi, \pi]$.

Figure 2.5 refers to the summation of Chern number phase diagrams of all bands with respect to rotation parameters θ_1, θ_2 and indicates boundaries of the protocol at some rotation parameters. $\sum_n C_n = 0$ corresponds to the green colour in the phase diagram.

2.2.2 The Second Split-Step Quantum Walk Protocol

The second split-step quantum protocol in this chapter can be denoted by using the following unitary operators that describe coin rotations and translation over the two-dimensional lattice. The main difference from the first model is that coins dictated the motion the direction of one Cartesian coordinate and non-local rotation is made of y-directions.

1. Alice tosses the first coin along the x-axis;

$$\hat{C}_A = e^{-i\theta_1 \sigma_x^{(A)}/2} \tag{2.21}$$

2. The conditional shift operator is defined on the walker along the x-axis;

$$\hat{S}_{A_x} = \sum_x \left(|x+1\rangle \langle x| \otimes |0\rangle_A \langle 0|_A + |x-1\rangle \langle x| \otimes |1\rangle_A \langle 1|_A \right) \tag{2.22}$$

3. Bob tosses the coin along the x-axis;

$$\hat{C}_B = e^{-i\theta_2 \sigma_x^{(B)}/2} \tag{2.23}$$

4. After the coin tossing, the shift operator along the y-axis is;

$$\hat{S}_{B_y} = \sum_y \left(|y+1\rangle \langle y| \otimes |0\rangle_B \langle 0|_B + |y-1\rangle \langle y| \otimes |1\rangle_B \langle 1|_B \right) \tag{2.24}$$

5. A non-local(collective) coin operator is introduced along the y direction;

$$\hat{C}_{AB} = e^{-i\theta_3 \sigma_y^{(A)} \otimes \sigma_y^{(B)}/2} \tag{2.25}$$

6. Followed by the non-local coin operation, a displacement is made in two Cartesian directions;

$$\hat{S}_{A_xB_y} = \sum_{x,y} |x+1, y+1\rangle \langle x, y| \otimes |00\rangle_{AB} \langle 00|_{AB} + |x+1, y-1\rangle \langle x, y| \otimes |01\rangle_{AB} \langle 01|_{AB} + |x-1, y+1\rangle \langle x, y| \otimes |10\rangle_{AB} \langle 10|_{AB} + |x-1, y-1\rangle \langle x, y| \otimes |11\rangle_{AB} \langle 11|_{AB} \quad (2.26)$$

As seen in the split-step quantum walk protocols above, displacements corresponding to coin's spin state are made in the same direction. The one-step split-step quantum walk protocol can be represented as the following,

$$\hat{U}^{(2)} = \hat{S}_{A_xB_y} \hat{C}_{AB} \hat{S}_{B_y} \hat{C}_B \hat{S}_{A_x} \hat{C}_A \quad (2.27)$$

$$\hat{U}^{(2)} = \int_{-\frac{\pi}{2}}^{\frac{\pi}{2}} \int_{-\frac{\pi}{2}}^{\frac{\pi}{2}} e^{-i\epsilon_n(k_x,k_y)} \left|\phi_n(k_x, k_y)\right\rangle \left\langle\phi_n(k_x, k_y)\right| dk_x dk_y \otimes \left|k_x, k_y\right\rangle \left\langle k_x, k_y\right| \quad (2.28)$$

Chern number phase diagram of the protocol can be found by using Eq. (1.31) which describes the numerical calculation of Chern number on discretized first Brillouin zone.

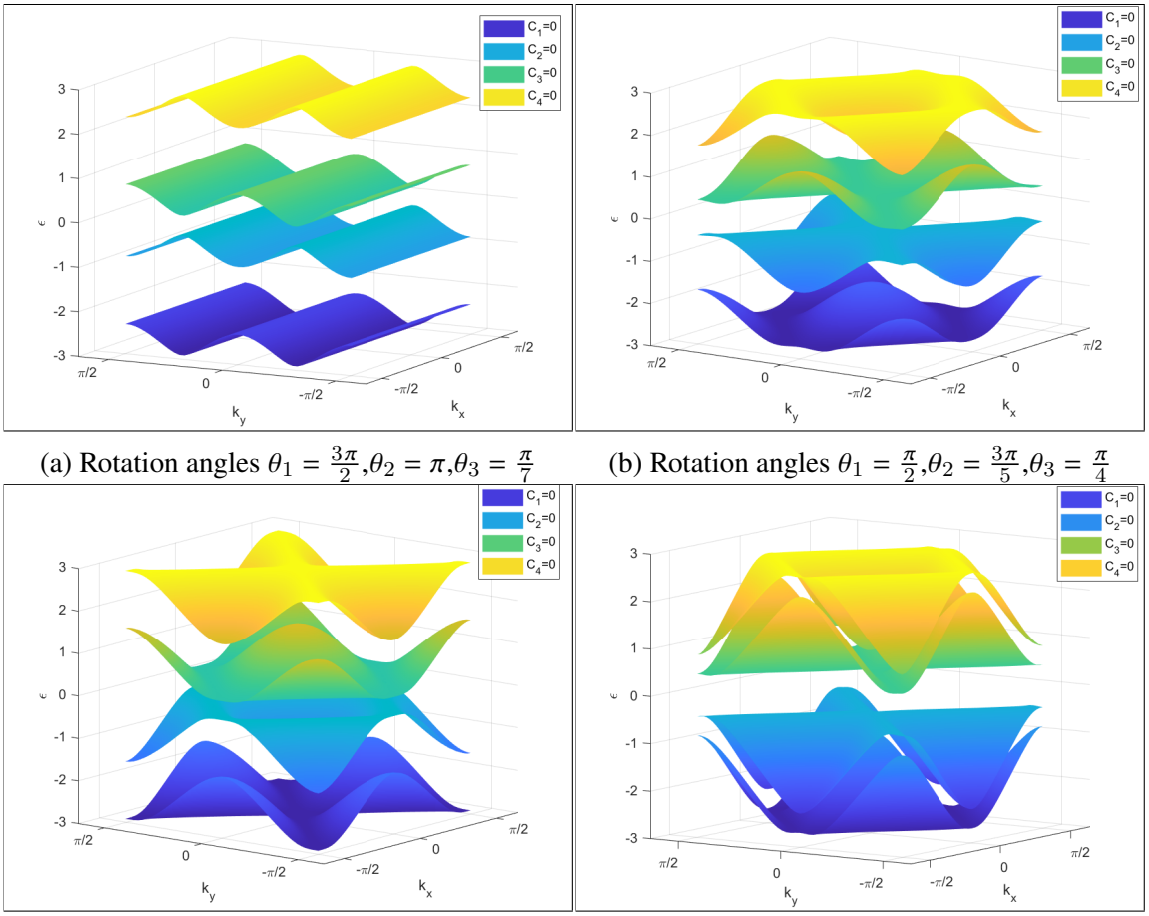

(a) Rotation angles $\theta_1 = \frac{3\pi}{2}$,$\theta_2 = \pi$,$\theta_3 = \frac{\pi}{7}$

(b) Rotation angles $\theta_1 = \frac{\pi}{2}$,$\theta_2 = \frac{3\pi}{5}$,$\theta_3 = \frac{\pi}{4}$

(c) Rotation angles $\theta_1 = \frac{3\pi}{2}$, $\theta_2 = \frac{\pi}{2}$, $\theta_3 = \frac{\pi}{7}$

(d) Rotation angles $\theta_1 = \frac{2\pi}{7}$,$\theta_2 = \frac{\pi}{5}$,$\theta_3 = \frac{3\pi}{11}$

Figure 2.6: The quasi-energy spectrum of the second split-step quantum walk protocol for various rotation angles θ_1,θ_2, and θ_3 in first Brillouin zone $k_{x,y} \in [-\pi/2, \pi/2]$.

Figure 2.6 represents the quasi-energy spectrum of the protocol and shows that Chern numbers are zero for each band for various rotation parameters θ_1, θ_2, and θ_3.

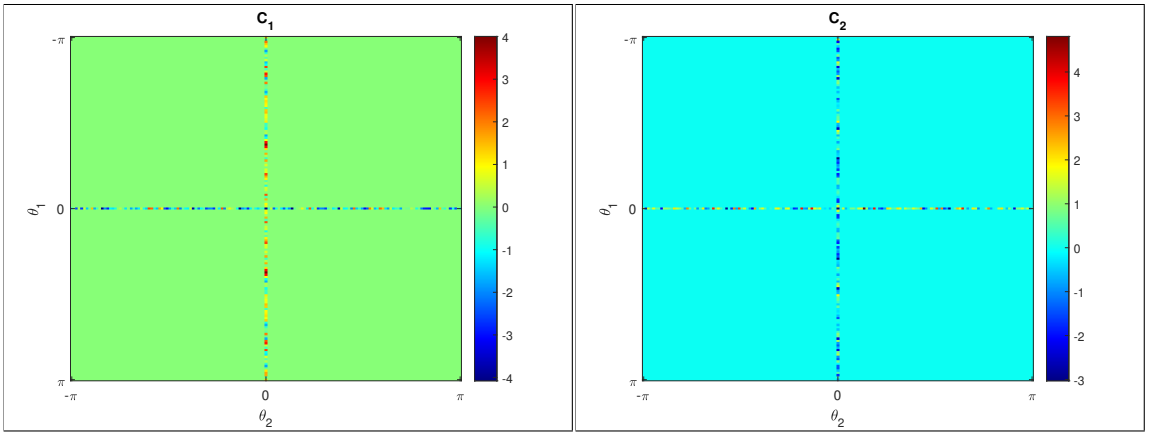

(a) Rotation angle $\theta_3 = \frac{\pi}{4}$ (b) Rotation angle $\theta_3 = \frac{\pi}{4}$

Figure 2.7: Chern number phase diagram of the second split-step quantum walk protocol is obtained with constant rotation parameter θ_3 for the ground state and the first excited state in the interval of $\theta_1, \theta_2 \in [-\pi, \pi]$.

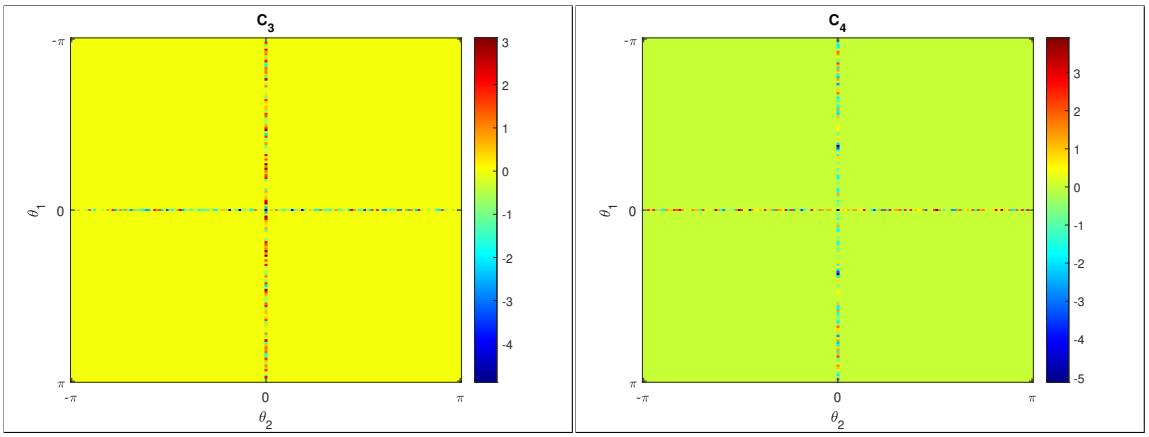

(a) Rotation angle $\theta_3 = \frac{\pi}{4}$ (b) Rotation angle $\theta_3 = \frac{\pi}{4}$

Figure 2.8: Chern number phase diagram of the second split-step quantum walk protocol is obtained with constant rotation parameter θ_3 for the second excited state and the third excited state in the interval of $\theta_1, \theta_2 \in [-\pi, \pi]$.

Figures 2.7-2.8 correspond to Chern number phase diagram and clearly indicate that each band is characterized by integer of 0 for constant rotation parameter θ_3 except boundaries of the systems.

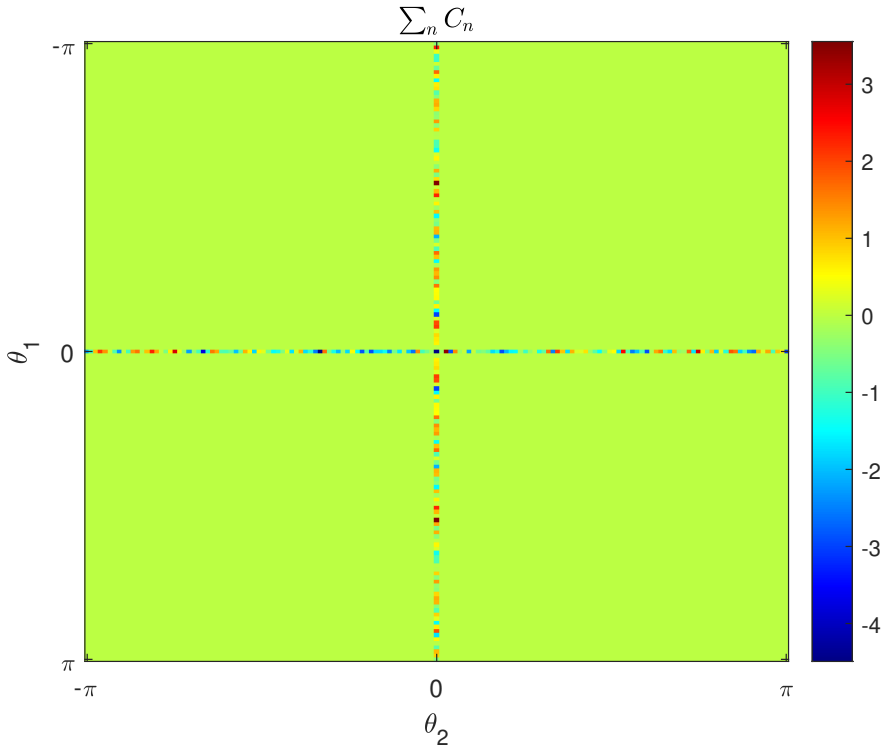

Figure 2.9: Summation of Chern number phase diagrams of all bands with constant rotation parameter $\theta_3 = \frac{\pi}{4}$ is plotted in the interval of $\theta_1, \theta_2 \in [-\pi, \pi]$.

Figure 2.9 refers to the summation of Chern numbers of all bands with constant rotation parameter θ_3 and indicates that the second split-step quantum walk protocol exhibits trivial topology except boundaries. The green colour corresponds to $\sum_n C_n = 0$.

2.2.3 The Third Split-Step Quantum Walk Protocol

This protocol is introduced by choosing the rotation direction of the non-local operator along the z and y directions, respectively. It can be defined step by step as in the other protocols,

1. Alice tosses the coin in the direction of x,

$$\hat{C}_A = e^{-i\theta_1 \sigma_x^{(A)}/2} \tag{2.29}$$

2. The spin-dependent shift operator is introduced,

$$\hat{S}_{A_y} = \sum_y \left(|y+1\rangle \langle y| \otimes |0\rangle_A \langle 0|_A + |y-1\rangle \langle y| \otimes |1\rangle_A \langle 1|_A \right) \tag{2.30}$$

3. Bob tosses the coin in the direction x,

$$\hat{C}_B = e^{-i\theta_2 \sigma_x^{(B)}/2} \tag{2.31}$$

4. After the coin tossing, the shift operator along the y- axis is;

$$\hat{S}_{B_x} = \sum_x \left(|x+1\rangle \langle x| \otimes |0\rangle_B \langle 0|_B + |x-1\rangle \langle x| \otimes |1\rangle_B \langle 1|_B \right) \tag{2.32}$$

5. Non-local(collective) coin operator in the directions of z and y is introduced the following;

$$\hat{C}_{AB} = e^{-i\theta_3 \sigma_z^{(A)} \otimes \sigma_y^{(B)}/2} \tag{2.33}$$

6. Followed by the non-local coin operator, a displacement is made in two Cartesian directions;

$$\begin{aligned} \hat{S}_{A_x B_y} = \sum_{x,y} & |x+1, y+1\rangle \langle x, y| \otimes |00\rangle_{AB} \langle 00|_{AB} + |x+1, y-1\rangle \langle x, y| \otimes |01\rangle_{AB} \langle 01|_{AB} \\ & + |x-1, y+1\rangle \langle x, y| \otimes |10\rangle_{AB} \langle 10|_{AB} + |x-1, y-1\rangle \langle x, y| \otimes |11\rangle_{AB} \langle 11|_{AB} \end{aligned} \tag{2.34}$$

The evolution operator of the protocol is then,

$$\hat{U}^{(3)} = \hat{S}_{A_x B_y} \hat{C}_{AB} \hat{S}_{B_x} \hat{C}_B \hat{S}_{A_y} \hat{C}_A \tag{2.35}$$

$$\hat{U}^{(3)} = \int_{-\frac{\pi}{2}}^{\frac{\pi}{2}} \int_{-\frac{\pi}{2}}^{\frac{\pi}{2}} e^{-i\epsilon_n(k_x,k_y)} \left|\phi_n(k_x,k_y)\right\rangle \left\langle\phi_n(k_x,k_y)\right| dk_x dk_y \otimes \left|k_x,k_y\right\rangle \left\langle k_x,k_y\right| \tag{2.36}$$

The numerical analysis of the third split-step quantum walk can be obtained to implement the topological properties of the system.

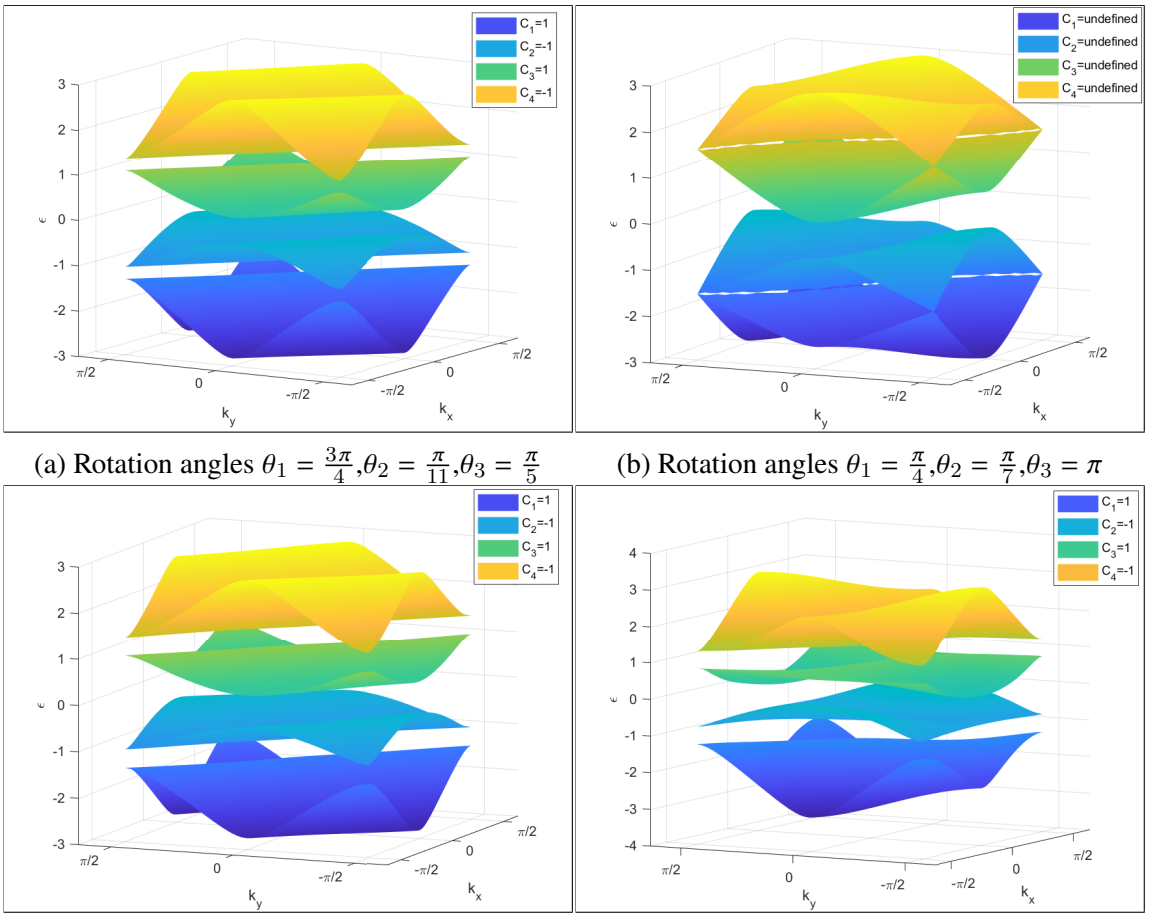

(a) Rotation angles $\theta_1 = \frac{3\pi}{4}$,$\theta_2 = \frac{\pi}{11}$,$\theta_3 = \frac{\pi}{5}$

(b) Rotation angles $\theta_1 = \frac{\pi}{4}$,$\theta_2 = \frac{\pi}{7}$,$\theta_3 = \pi$

(c) Rotation angles $\theta_1 = \frac{3\pi}{4}$, $\theta_2 = \frac{\pi}{7}$, $\theta_3 = \frac{\pi}{4}$

(d) Rotation angles $\theta_1 = \frac{2\pi}{5}$,$\theta_2 = \frac{-\pi}{3}$,$\theta_3 = \frac{\pi}{2}$

Figure 2.10: The quasi-energy spectrum of the third split-step quantum walk protocol for various rotation angles θ_1,θ_2, and θ_3 in first Brillouin zone $k_{x,y} \in [-\pi/2, \pi/2]$.

Figure 2.10 indicates the quasi-energy spectrum of the third-split step quantum walk protocol and associates each band with Chern number. In (b), Chern numbers are undefined, since there are bands touching at these rotation parameters. We are keeping in mind that the numerical method is valid for non-degenerate systems.

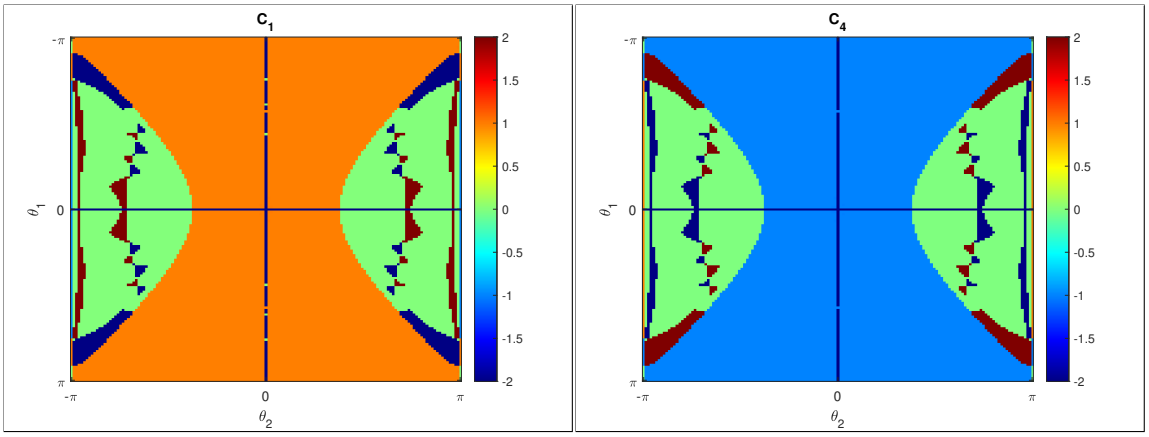

(a) Rotation angle $\theta_3 = \frac{\pi}{4}$ (b) Rotation angle $\theta_3 = \frac{\pi}{4}$

Figure 2.11: Chern number phase diagram of the third split-step quantum walk protocol is plotted for the ground state and the third excited state in the interval $\theta_1, \theta_2 \in [-\pi, \pi]$.

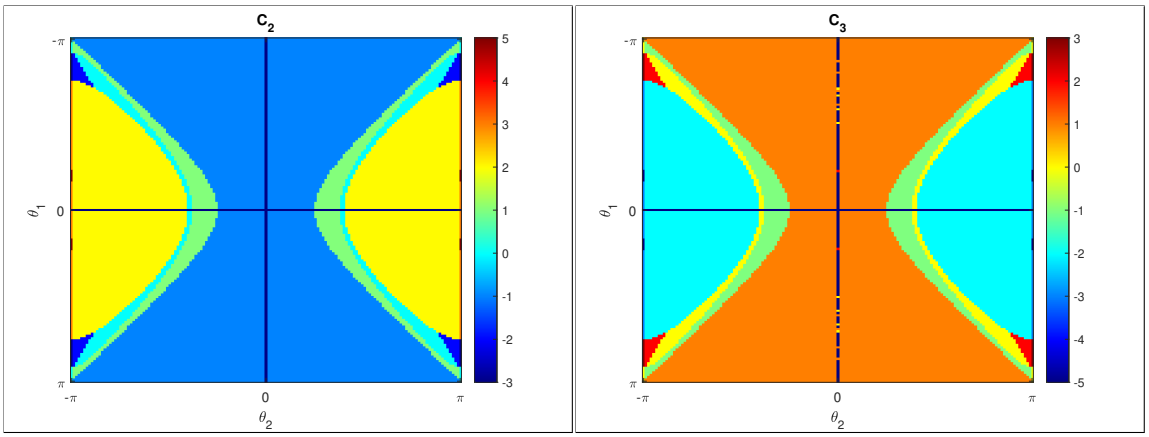

(a) Rotation angle $\theta_3 = \frac{\pi}{4}$ (b) Rotation angle $\theta_3 = \frac{\pi}{4}$

Figure 2.12: Chern number phase diagram of the third split-step quantum walk protocol is plotted for the first excited state and the second excited state in the interval $\theta_1, \theta_2 \in [-\pi, \pi]$.

Figures 2.11-2.12 shows how Chern number of each quasi-energy band with constant rotation parameter θ_3 is associated with respect to parameters θ_1, θ_2. Chern number phase diagrams are more consistent than the phase diagrams of the first split-step quantum walk protocol. The protocol with constant rotation parameter θ_3 is mostly characterized with the integers of $-2, -1, 0, 1, 2$.

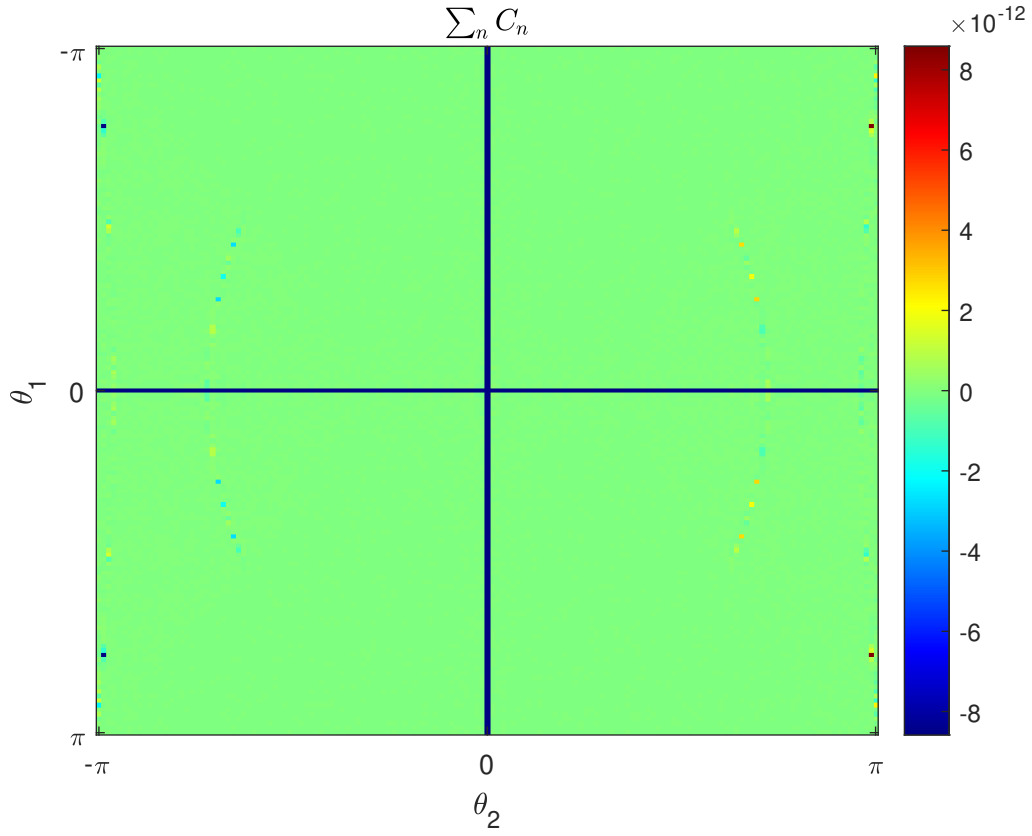

Figure 2.13: Summation of Chern number phase diagrams of all bands with constant rotation parameter $\theta_3 = \frac{\pi}{4}$ is obtained in the interval of $\theta_1, \theta_2 \in [-\pi, \pi]$.

As expected from above Figures 2.11-2.12, Figure 2.13 has a clear interpretation of the summation of Chern number phase diagram of each band. Except for the boundaries, it is seen clearly that $\sum_n C_n = 0$.

2.3 Coin-Coin Entanglement of Topological Quantum Walks

This section investigates coin-coin entanglement of the quantum walk protocols governed by two coins since each protocol exhibits different topological properties in momentum space. Entanglement is an essential property of quantum physics that does not occur in classical physics. Entanglement emerges when particles are correlated in such a way the state of the whole system cannot be described independently of the state of each particle. In a bipartite system, the entanglement is measured by von Neumann entropy which provides the amount of entanglement(von Neumann, 1955). Since coins are entangled by non-local coin operators in our protocols, the state of one coin cannot be known independently of the other coin. For a given quantum walk protocol,

$$\hat{U}^{(n)} = \int_{-\frac{\pi}{2}}^{\frac{\pi}{2}} \int_{-\frac{\pi}{2}}^{\frac{\pi}{2}} e^{-i\epsilon_n(k_x,k_y)} \left|\phi_n(k_x,k_y)\right\rangle \left\langle\phi_n(k_x,k_y)\right| dk_x dk_y \otimes \left|k_x,k_y\right\rangle \left\langle k_x,k_y\right| \quad (2.37)$$

where n corresponds to the band index. The spinor part of the eigenstates in Eq. (2.37) can be used to deduce coin-coin entanglement of the protocols. To obtain coin-coin entanglement for a particular state of the evolution operator, one may use the density matrix of the current state.

$$\rho_{AB}^{(n)} = \left|\phi_n(k_x,k_y)\right\rangle \left\langle\phi_n(k_x,k_y)\right| \quad (2.38)$$

Then, partial trace operator is introduced to obtain the reduced density matrix of each coin the following way,

$$\begin{aligned} \rho_A^{(n)} &= \mathrm{Tr}_B(\rho_{AB}^{(n)}) \\ \rho_B^{(n)} &= \mathrm{Tr}_A(\rho_{AB}^{(n)}) \end{aligned} \quad (2.39)$$

Since the eigenstates of the evolution operator correspond to a pure entangled state, the entropy of entanglement can be obtained for each coin A and B the following,

$$\begin{aligned} S^{(n)}(A) &= -\operatorname{Tr}\left(\rho_A^{(n)} \log_2(\rho_A^{(n)})\right) \\ S^{(n)}(B) &= -\operatorname{Tr}\left(\rho_B^{(n)} \log_2(\rho_B^{(n)})\right) \end{aligned} \tag{2.40}$$

It is obvious that $S^{(n)}(A) = S^{(n)}(B)$. Thus, it is sufficient to obtain and analyze only one coin's entropy of entanglement in momentum space.

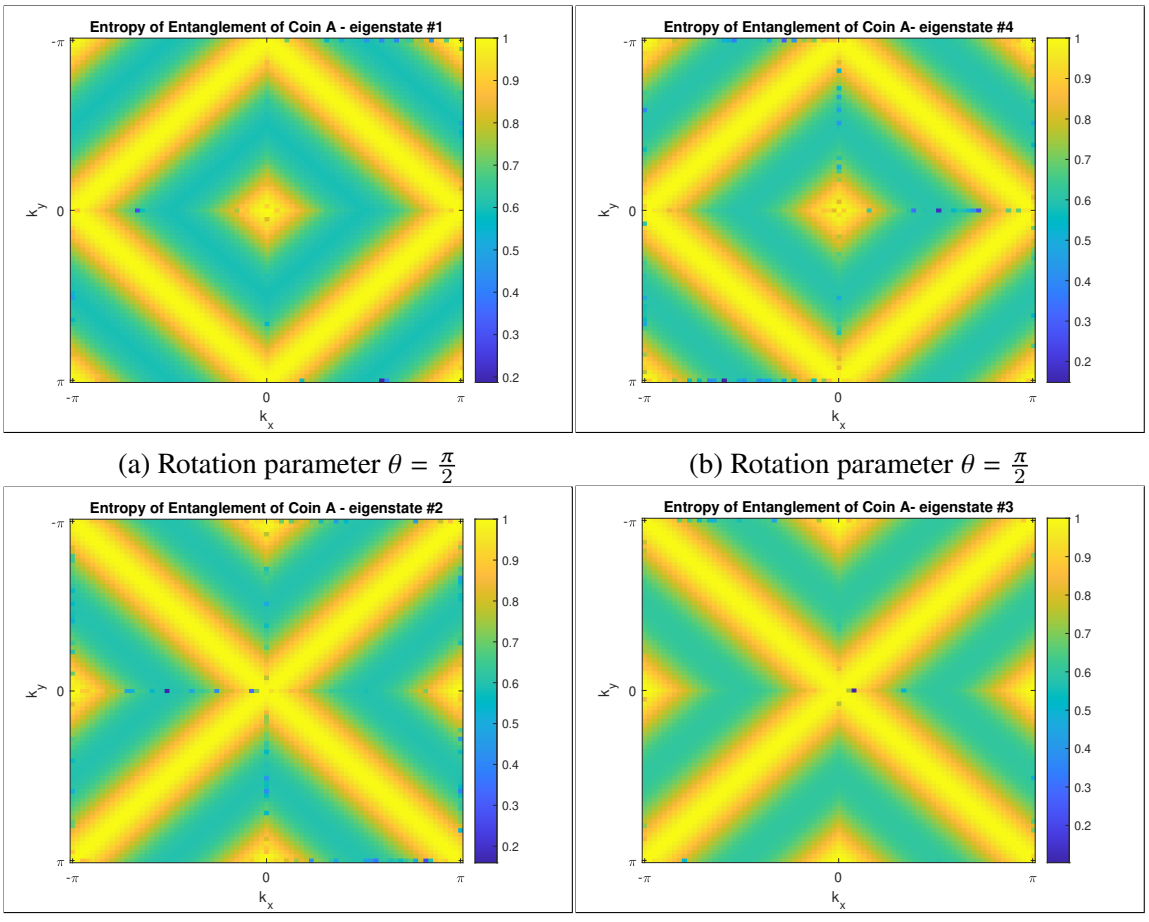

(a) Rotation parameter $\theta = \frac{\pi}{2}$

(b) Rotation parameter $\theta = \frac{\pi}{2}$

(c) Rotation parameter $\theta = \frac{\pi}{2}$

(d) Rotation parameter $\theta = \frac{\pi}{2}$

Figure 2.14: The entropy of entanglement of coin A for the simple quantum walk protocol governed by two coins at given rotation parameter $\theta = \frac{\pi}{2}$ is obtained in the interval of $(k_x, k_y) \in [-\pi, \pi]$.

Figure 2.14 corresponds to the entropy of entanglement of the quantum walk protocol studied in section 2.1 and indicates how decoupling occurs for eigenstates of the system. Since the quantum walk is effectively separated into one-dimensional walks in position space, Chern numbers are undefined. Also, the entropies of entanglement are maximized along the diagonal points since the walker is dictated to translate along x, y directions diagonally.

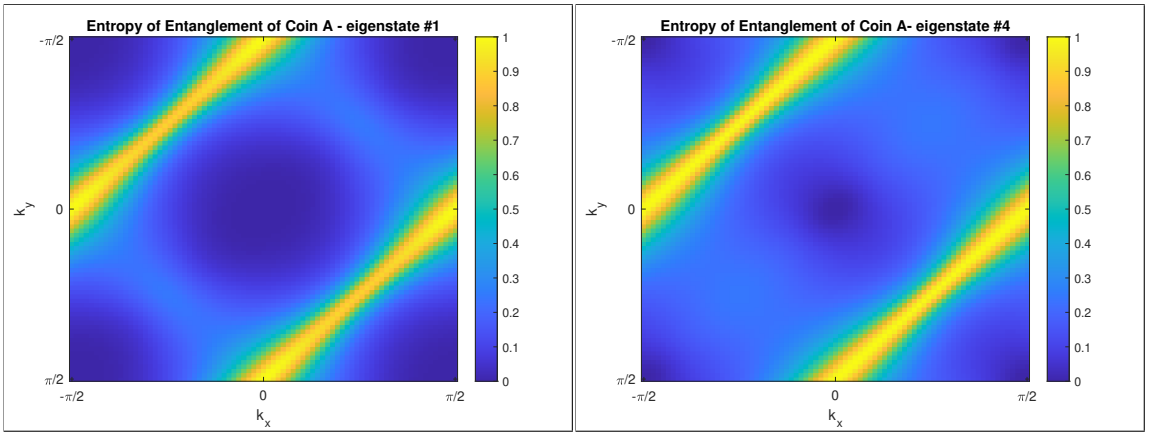

(a) $\theta_1 = \frac{\pi}{3}$, $\theta_2 = \frac{\pi}{2}$,$\theta_3 = \frac{\pi}{4}$ (b) $\theta_1 = \frac{\pi}{3}$, $\theta_2 = \frac{\pi}{2}$,$\theta_3 = \frac{\pi}{4}$

(c) $\theta_1 = \frac{\pi}{3}$, $\theta_2 = \frac{\pi}{2}$,$\theta_3 = \frac{\pi}{4}$ (d) $\theta_1 = \frac{\pi}{3}$, $\theta_2 = \frac{\pi}{2}$,$\theta_3 = \frac{\pi}{4}$

Figure 2.15: The entropy of entanglement of coin A for the first split-step quantum walk protocol in the interval of $(k_x, k_y) \in [-\pi/2, \pi/2]$.

Figure 2.15 represents the entropy of entanglement of the first split-step quantum walk protocol studied in section 2.2.1 for various rotation parameters. In (a,b), the entropy of entanglement is maximized along the diagonal points of (k_x, k_y). However, in (c,d), the entropy of entanglement is nearly the maximum at each point of (k_x, k_y) except boundary points and $(0, 0)$ points. At these rotation parameters, Chern number of each band corresponds to $C_1 = 0$, $C_2 = 2$, $C_3 = -2$, and $C_4 = 0$.

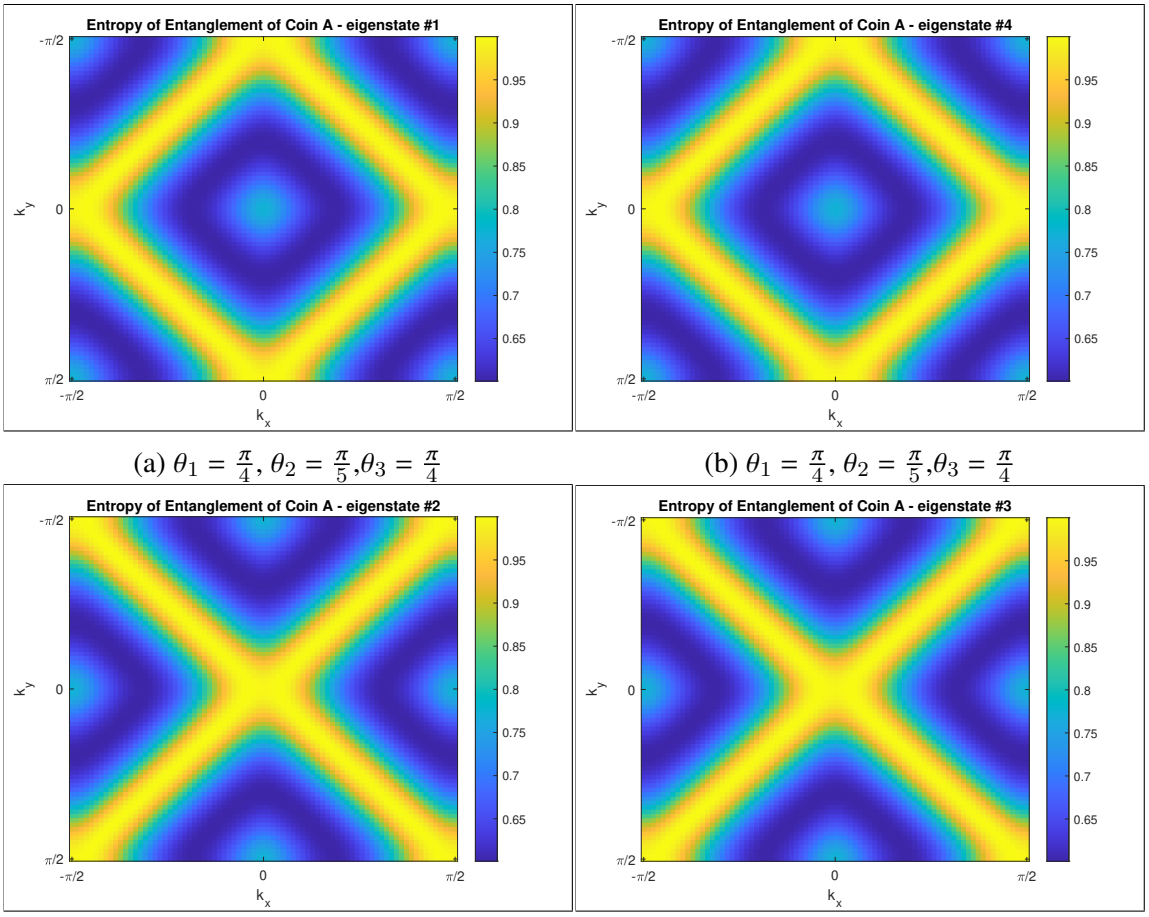

(a) $\theta_1 = \frac{\pi}{4}$, $\theta_2 = \frac{\pi}{5}$,$\theta_3 = \frac{\pi}{4}$

(b) $\theta_1 = \frac{\pi}{4}$, $\theta_2 = \frac{\pi}{5}$,$\theta_3 = \frac{\pi}{4}$

(c) $\theta_1 = \frac{\pi}{4}$, $\theta_2 = \frac{\pi}{5}$,$\theta_3 = \frac{\pi}{4}$

(d) $\theta_1 = \frac{\pi}{4}$, $\theta_2 = \frac{\pi}{5}$,$\theta_3 = \frac{\pi}{4}$

Figure 2.16: The entropy of entanglement of coin A for the second split-step quantum walk protocol in the interval of $(k_x, k_y) \in [-\pi/2, \pi/2]$.

Figure 2.16 comprises the entropy of entanglement of the second-split step protocol studied in Section 2.2.2 and shows how the entropy of entanglement of the coins is related to rotation parameters. In this protocol, the entropy of entanglement is maximized along the diagonal points of (k_x, k_y) similar to Figure 2.14, although the decoupling does not occur. As seen from Figures 2.7-2.8, Chern numbers are zero for each band.

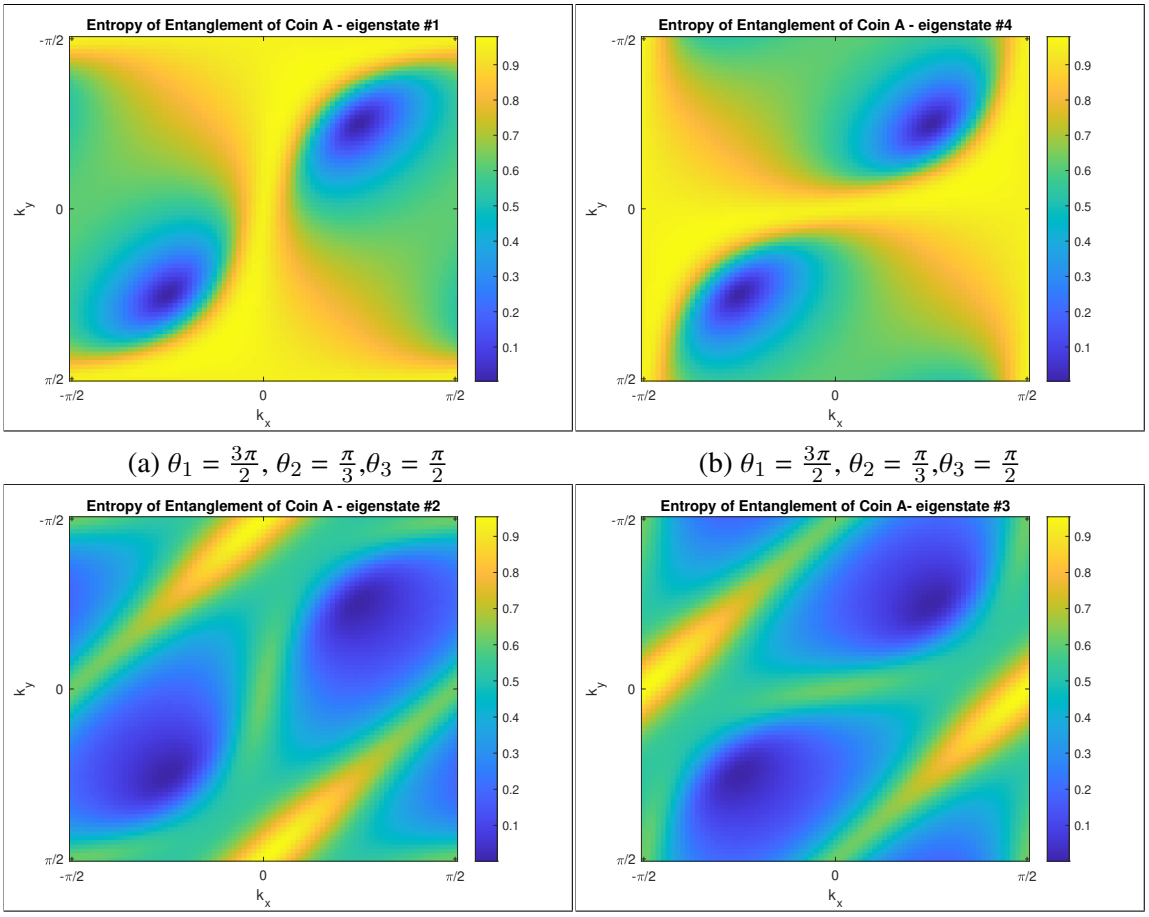

(a) $\theta_1 = \frac{3\pi}{2}$, $\theta_2 = \frac{\pi}{3}$,$\theta_3 = \frac{\pi}{2}$

(b) $\theta_1 = \frac{3\pi}{2}$, $\theta_2 = \frac{\pi}{3}$,$\theta_3 = \frac{\pi}{2}$

(c) $\theta_1 = \frac{3\pi}{2}$, $\theta_2 = \frac{\pi}{3}$,$\theta_3 = \frac{\pi}{2}$

(d) $\theta_1 = \frac{3\pi}{2}$, $\theta_2 = \frac{\pi}{3}$,$\theta_3 = \frac{\pi}{2}$

Figure 2.17: The entropy of entanglement of coin A for the third split-step quantum walk protocol in the interval of $(k_x, k_y) \in [-\pi/2, \pi/2]$.

Figure 2.17 refers to the entropy of entanglement of the third split-step protocol studied in Section 2.2.3 and implies how coins are correlated at given rotation parameters. Unlike the other protocols, the distribution of the entropy of entanglement is not maximized to a specific direction along (k_x, k_y) points at given rotation parameters. Chern number of each band corresponds to $C_1 = 1$, $C_2 = -1$, $C_3 = 1$, and $C_4 = -1$ at these rotation parameters.

CHAPTER 3

CONCLUSION

In this thesis, we extended the quantum walks by adding one more coin and then, investigated their topological and coin-coin entanglement properties. We first defined a simple quantum walk governed by a single non-local(collective) two-coin operator and followed by a translation operator along two spatial directions. In this protocol, we concluded that the walk operator is reduced effectively into one-dimensional quantum walks due to the decoupling of the eigenbasis of the coin's subspace. Therefore, the simple protocol can possess the winding numbers instead of Chern numbers. Then we introduced and studied the split-step quantum walk protocols governed by two coins in a two-dimensional space. In these split-step protocols, we did not encounter a decoupling, since local quantum walks effectively broke the spatial symmetry. In the first split-step protocol, we obtained Chern number phase diagram with constant rotation parameter $\theta_3 = \frac{\pi}{4}$ and deduced that the protocol is mostly characterized by integers of $-2, 0, 2$ as a function of θ_1,θ_2. The second split-step protocol, unlike the first protocol, exhibited trivial topology for constant rotation parameter $\theta_3 = \frac{\pi}{4}$ and its Chern number phase diagram is obtained with respect to θ_1, θ_2 parameters. The third split-step protocol has been introduced in a similar fashion, but the difference in its non-local coin operation gave rise to more different topological properties than the first protocol. We have concluded that the third protocol with constant rotation parameter $\theta_3 = \frac{\pi}{4}$ is mostly characterized by integers of $-2, -1, 0, 1, 2$ as a function of rotation parameters θ_1, θ_2. Then, we obtained the coin-coin entanglement of each quantum walk protocol with respect to rotation parameters. The coin-coin entanglement in the simple quantum walk is mostly maximized in diagonal directions of lattice points. The decoupling of the simple walk into one-dimensional quantum walks can be the reason for this maximization along the diagonal directions. The coin-coin entanglement in the first split-step protocols is widely different among the current eigenstates. At given rotation parameters, the entropy of entanglement of coin A at the first excited state and at the second excited state is effectively maximized, except for boundaries of the Brillouin zone and $(0, 0)$ point. Chern numbers associated with these current eigenstates are integers of $C_1 = 0$, $C_2 = 2$, $C_3 = -2$, and $C_4 = 0$. Then, we obtained the coin-coin entanglement of the second split-step quantum walk protocol(trivial topology) at given rotation parameters and associated that the reason for diagonal maximization of the entropy of entanglement can stem from the conditional

translation operators along the same direction governed by each different coin. We lastly investigated the entropy of entanglement of the third split-step quantum walk protocol at given rotation parameters. The coin-coin entanglement of the third protocol indicated that the maximization of the entropy of entanglement in a specific direction does not occur at given rotation parameters. Chern numbers associated with given rotation parameters correspond to $C_1 = 1$, $C_2 = -1$,$C_3 = 1$, and $C_4 = -1$.

REFERENCES

Dorit Aharonov, Andris Ambainis, Julia Kempe, and Umesh Vazirani. 2001. Quantum Walks on Graphs. In *Proceedings of the Thirty-Third Annual ACM Symposium on Theory of Computing (STOC '01)*. Association for Computing Machinery, New York, NY, USA, 50–59. https://doi.org/10.1145/380752.380758

Y Aharonov, L Davidovich, and N Zagury. 1993. PHYSICAL REVIEW A VOLUME 48, NUMBER 2 Quantum random walks.

Andris Ambainis, Eric Bach, Ashwin Nayak, Ashvin Vishwanath, and John Watrous. 2001. One-Dimensional Quantum Walks. In *Proceedings of the Thirty-Third Annual ACM Symposium on Theory of Computing (STOC '01)*. Association for Computing Machinery, New York, NY, USA, 37–49. https://doi.org/10.1145/380752.380757

M. A. Broome, A. Fedrizzi, B. P. Lanyon, I. Kassal, A. Aspuru-Guzik, and A. G. White. 2010. Discrete Single-Photon Quantum Walks with Tunable Decoherence. *Phys. Rev. Lett.* 104 (Apr 2010), 153602. Issue 15. https://doi.org/10.1103/PhysRevLett.104.153602

Andrew M. Childs, Richard Cleve, Enrico Deotto, Edward Farhi, Sam Gutmann, and Daniel A. Spielman. 2003. Exponential Algorithmic Speedup by a Quantum Walk. In *Proceedings of the Thirty-Fifth Annual ACM Symposium on Theory of Computing (STOC '03)*. Association for Computing Machinery, New York, NY, USA, 59–68. https://doi.org/10.1145/780542.780552

A. Einstein. 1905. Über die von der molekularkinetischen Theorie der Wärme geforderte Bewegung von in ruhenden Flüssigkeiten suspendierten Teilchen. *Annalen der Physik* 322, 8 (1905), 549–560. https://doi.org/10.1002/andp.19053220806 arXiv:https://onlinelibrary.wiley.com/doi/pdf/10.1002/andp.19053220806

Edward Farhi and Sam Gutmann. 1998. Quantum computation and decision trees. *Phys. Rev. A* 58 (Aug 1998), 915–928. Issue 2. https://doi.org/10.1103/PhysRevA.58.915

Takahiro Fukui, Yasuhiro Hatsugai, and Hiroshi Suzuki. 2005. Chern numbers in discretized Brillouin zone: Efficient method of computing (spin) Hall conductances. *Journal of the Physical Society of Japan* 74 (6 2005), 1674–1677. Issue 6. https://doi.org/10.1143/JPSJ.74.1674

D. Hsieh, D. Qian, L. Wray, Y. Xia, Y. S. Hor, R. J. Cava, and M. Z. Hasan. 2009. A topological Dirac insulator in a quantum spin Hall phase (experimental realization of a 3D Topological Insulator). arXiv:cond-mat.mes-hall/0910.2420

Michal Karski, Leonid Förster, Jai-Min Choi, Andreas Steffen, Wolfgang Alt, Dieter Meschede, and Artur Widera. 2009. Quantum Walk in Position Space with Single Optically Trapped Atoms. *Science* 325, 5937 (2009), 174–177. https://doi.org/10.1126/science.1174436 arXiv:https://www.science.org/doi/pdf/10.1126/science.1174436

J Kempe. 2003. Quantum random walks: An introductory overview. *Contemporary Physics* 44, 4 (2003), 307–327. https://doi.org/10.1080/0010715103100011077 6 arXiv:https://doi.org/10.1080/00107151031000110776

J. Kempe. 2005. Discrete Quantum Walks Hit Exponentially Faster. *Probab. Theory Relat. Fields* 133 (2005), 215–235. https://doi.org/10.1007/s00440-004-0423-2

Takuya Kitagawa. 2012. Topological phenomena in quantum walks: Elementary introduction to the physics of topological phases. *Quantum Information Processing* 11 (10 2012), 1107–1148. Issue 5. https://doi.org/10.1007/s11128-012-0425-4

T. Kitagawa, M. A. Broome, A. Fedrizzi, M. S. Rudner, E. Berg, I. Kassal, A. Aspuru-Guzik, E. Demler, and A. G. White. 2012. Observation of topologically protected bound states in photonic quantum walks. *Nat. Commun.* 3, 1 (2012), 882.

Takuya Kitagawa, Mark S. Rudner, Erez Berg, and Eugene Demler. 2010. Exploring Topological Phases With Quantum Walks. (3 2010). https://doi.org/10.1103/PhysRevA.82.033429

K. v. Klitzing, G. Dorda, and M. Pepper. 1980. New Method for High-Accuracy Determination of the Fine-Structure Constant Based on Quantized Hall Resistance. *Phys. Rev. Lett.* 45 (Aug 1980), 494–497. Issue 6. https://doi.org/10.1103/PhysRevLett.45.494

Markus Koenig, Steffen Wiedmann, Christoph Bruene, Andreas Roth, Hartmut Buhmann, Laurens W. Molenkamp, Xiao-Liang Qi, and Shou-Cheng Zhang. 2007. Quantum Spin Hall Insulator State in HgTe Quantum Wells. (10 2007). https://doi.org/10.1126/science.1148047

Neil B. Lovett, Sally Cooper, Matthew Everitt, Matthew Trevers, and Viv Kendon. 2010. Universal quantum computation using the discrete-time quantum walk. *Phys. Rev. A* 81 (Apr 2010), 042330. Issue 4. https://doi.org/10.1103/PhysRevA.81.042330

Lawrence Page, Sergey Brin, Rajeev Motwani, and Terry Winograd. 1999. The PageRank Citation Ranking : Bringing Order to the Web. In *The Web Conference*.

K. Pearson. 1905. The Problem of the Random Walk. *Nature* 72 (1905), 294. https://doi.org/10.1038/072294b0

Neil Shenvi, Julia Kempe, and K. Birgitta Whaley. 2003. Quantum random-walk search algorithm. *Phys. Rev. A* 67 (May 2003), 052307. Issue 5. https://doi.org/10.1103/PhysRevA.67.052307

P.W. Shor. 1994. Algorithms for quantum computation: discrete logarithms and factoring. In *Proceedings 35th Annual Symposium on Foundations of Computer Science*. 124–134. https://doi.org/10.1109/SFCS.1994.365700

F. Spitzer. 1964. *Principles of Random Walk*. Vol. 34. Springer.

D. J. Thouless, M. Kohmoto, M. P. Nightingale, and M. den Nijs. 1982. Quantized Hall Conductance in a Two-Dimensional Periodic Potential. *Phys. Rev. Lett.* 49 (Aug 1982), 405–408. Issue 6. https://doi.org/10.1103/PhysRevLett.49.405

Salvador E. Venegas-Andraca. 2012. Quantum walks: a comprehensive review. (1 2012). https://doi.org/10.1007/s11128-012-0432-5

John von Neumann. 1955. *Mathematical Foundations of Quantum Mechanics*. Princeton University Press, Princeton.

Qin-Qin Wang, Xiao-Ye Xu, Wei-Wei Pan, Si-Jing Tao, Zhe Chen, Yong-Tao Zhan, Kai Sun, Jin-Shi Xu, Geng Chen, Yong-Jian Han, Chuan-Feng Li, and Guang-Can Guo. 2020. Robustness of entanglement as an indicator of topological phases in quantum walks. *Optica* 7 (1 2020), 53. Issue 1. https://doi.org/10.1364/optica.375388

L. Xiao, X. Zhan, Z. H. Bian, K. K. Wang, X. Zhang, X. P. Wang, J. Li, K. Mochizuki, D. Kim, N. Kawakami, W. Yi, H. Obuse, B. C. Sanders, and P. Xue. 2017. Observation of topological edge states in parity–time-symmetric quantum walks. *Nat. Phys.* 13, 11 (2017), 1117. https://doi.org/10.1038/nphys4204